

## Chapter 4. Tsunami Probability

ERIC L. GEIST, TOM PARSONS, URI S. TEN BRINK, AND HOMA J. LEE

*U.S. Geological Survey*

### Contents

1. Introduction
  2. Empirical Tsunami Probabilities
  3. Computational Tsunami Probabilities
  4. Uncertainties
  5. Summary
- References

### 1. Introduction

Evaluating the probability of tsunami occurrence is a crucial step in the assessment of tsunamis hazards. Deterministic tsunami hazard studies involve hydrodynamic modeling of tsunami propagation, runup, and inundation from a particular source, usually defined as the maximum credible earthquake, landslide, or another tsunami trigger. Scenario-based modeling such as this is useful in emergency planning, but transferring the modeling results to other applications, such as estimating risk, is difficult. Risk assessment relies heavily on determining the probability that a tsunami of a certain size will occur within a given time frame.

A tsunami hazard curve that plots tsunami size against probability for a given exposure time ( $T$ ) is a central concept in such analyses (Fig. 4.1). There are two ways in which a tsunami hazard curve can be used. The most common way is specifying a particular probability and exposure time of interest, and then determining the magnitude that a hazard variable (e.g., runup  $R$ ) that will be met or exceeded (Fig. 4.1a). An example of such an approach is flood hazard analysis for insurance applications in which the wave height and extent are determined for annualized probabilities ( $T=1$  yr.)  $P=0.01$  and  $P=0.002$  (Houston and Garcia, 1978). Alternatively, engineering applications may specify a risk tolerance value for a particular structure and use the hazard curve to determine the probability that that value will be met or exceeded during the exposure time (Fig. 4.1b). In addition to tsunami hazard curves for a particular site, probabilistic-based hazard assessment tools commonly include regional assessments (Rikitake and Aida, 1988; Geist and Parsons, 2006) and probabilistic inundation maps (Tsunami Pilot Study Working Group, 2006).

*The Sea*, Volume 15, edited by Eddie N. Bernard and Allan R. Robinson  
ISBN 978-0-674-03173-9 ©2009 by the President and Fellows of Harvard College

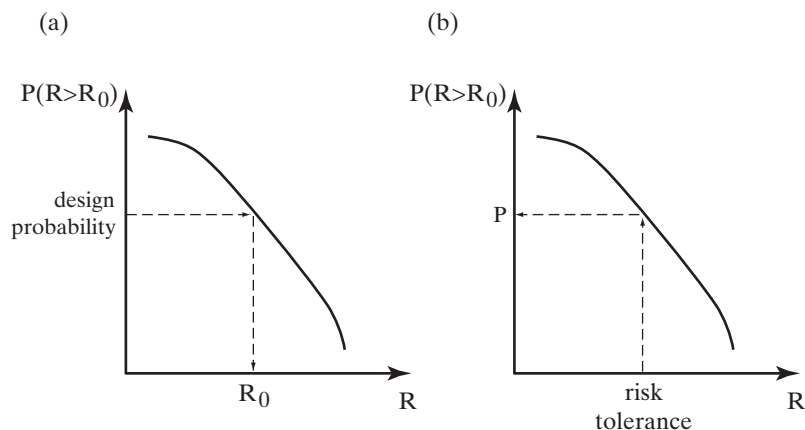


Fig. 4.1 – Schematic tsunami hazard curve showing different applications: (a) exceedance runup determined from design probability; (b) probability determined from risk tolerance.

In this paper we review techniques to determine tsunami probability using both empirical and computational approaches (Sections 2 and 3, respectively). Two distributions that form the basis for determining the probability of tsunamis (empirical) and their sources (computational) are the frequency-size distribution and the occurrence distribution of events in time. The former is nominally a power-law distribution, whereas the latter is often assumed to be an exponential distribution associated with a Poisson process. For the empirical analysis of tsunami observations at a particular coastal site, these assumptions greatly simplify the probability calculation: the probability ( $P$ ) that a tsunami of a certain size ( $R_0$ ) or greater will occur within time  $T$  is given by  $P = 1 - e^{-\lambda T}$ .  $\lambda$  is the long-term rate at which tsunamis of this size occur, which is given directly by the power-law size distribution  $\log(\lambda) \sim -\beta \log(R_0)$ , where  $\beta$  is the slope of the size distribution. One consequence of these assumptions is that for small values of  $\lambda T \ll 1$ ,  $P \approx \lambda T$ . There are, however, important deviations from these fundamental distributions and significant sources of uncertainty that are discussed in Section 2.

For most coastal locations, there is insufficient data to determine tsunami probability empirically. In these cases, probability is calculated using a combination of source specifications and numerical propagation models (Section 3). Aggregation of tsunami propagation results from all relevant sources, both near- and far-field, yield a tsunami hazard curve (Fig. 4.1) that should be equivalent to the empirical hazard curve, if there were sufficient historic data available. In addition to tsunami generation parameters, an important part of the source specification is defining the source probability: i.e., the inter-event distribution and the distribution of source sizes (e.g., seismic moment for earthquakes and volume for landslides). As part of the aggregation step of computing probabilities, various sources of uncertainty are also importantly included as we discuss in Section 4. To determine the probability of the largest tsunamis, methods to account for uncertainty become increasingly important. We briefly review methods to determine the probability of extreme events in Section 4, focusing on estimation techniques that define the tail of the size distribution for tsunamis (empirical approach) and their sources (computational approach).

## 2. Empirical Tsunami Probabilities

Tsunamis can be considered a stochastic process based on two essential characteristics: (1) once generated, tsunamis can propagate long distances such that many different sources in different tectonic and geologic environments can influence the tsunami hazard at a particular coastal location and (2) each type of source that generates tsunamis is itself characterized by a high degree of complexity and non-linear interactions. As a result, tsunami probabilities can be defined by the frequency distribution of sizes and the distribution of inter-event or waiting times. Nominally, the frequency-size distribution follows a power-law relationship and the inter-event times are that of a Poisson process, typical of many natural hazards (Daley and Vere-Jones, 2003; Sornette, 2004). Furthermore, these two fundamental distributions are inter-related in that the scaling of mean frequency with size is linked to the scaling of inter-event times (Corral, 2005b). Each of the fundamental distributions is discussed further below, including how the parameters that define the specific probability distributions can be empirically obtained.

### 2.1 Frequency-Size Distribution

It is important to first define the variable that defines the size of a tsunami. Although runup is the measurement most often associated with tsunamis, because it is defined as the wave height with respect to ambient sea level at the maximum inundation distance, runup will occur at different geographic locations for different tsunamis. Tide gauges, on the other hand, record wave amplitude at a fixed location (see Chapter 7). For most probability problems, comparisons are made over broad geographic regions that may include both runup and wave amplitude measurements. An exception is the development of probabilistic inundation maps at a given location (Tsunami Pilot Study Working Group, 2006). Throughout this study, we will refer to runup as the tsunami size or hazard variable, although this may include other amplitude measurements of tsunamis as well.

Like many other natural hazards, the frequency-runup distribution for tsunamis at a particular location tends to follow a power-law relationship (Burroughs and Tebbens, 2005):

$$\log[\dot{N}(R)] = \alpha - \beta \log(R), \quad (1)$$

where  $\dot{N}(R)$  is the annual frequency of tsunami runup  $R$  or larger and the empirical constants  $\alpha$  and  $\beta$  can be thought of as activity and scale parameters, respectively, that are determined from tsunami catalog data. The power-law nature of tsunamis indicates that there is no characteristic size and stems from the fundamental physics of the tsunami source (e.g., earthquakes, landslides) as explained by Sornette (2004). For empirical analysis, because catalogs will undersample below some size, we need to include a catalog-completeness threshold,  $R_t$ . This results in a Pareto distribution, for which the probability density function (pdf) is

$$\phi(R) = \frac{\beta(R_t)^\beta}{R^{(1+\beta)}}, \text{ for } R_t \leq R \quad (2)$$

and the complementary cumulative distribution function (ccdf) or survivor function is

$$\Phi(R) = \left(\frac{R_t}{R}\right)^\beta, \text{ for } R_t \leq R \quad (3)$$

(cf., Kagan, 2002a). Kagan (2002a) and Vere-Jones et al. (2001) also provide other modified Pareto distributions that have a soft taper for the roll-off parameterized by a corner runup  $R_c$ , which can be estimated using maximum likelihood techniques.

Moreover, because tsunami runup is size limited due to size limitations of the source, non-linear propagation, and wave-breaking effects near shore (e.g., Korycansky and Lynett, 2005), the Pareto distribution must be limited at large runup values. However, the limit and shape of the distribution tail are generally unclear. Burroughs and Tebbens (2001; 2005) suggest a truncated power-law relationship based on the value of the largest event (i.e, truncation of the pdf at  $R_x$ ) that is equivalent to the truncated Gutenberg-Richter (G-R) size distribution for earthquakes (Kagan, 2002a):

$$\phi(R) = \frac{\beta R_t^\beta R_x^\beta}{(R_x^\beta - R_t^\beta) R^{(1+\beta)}}, \text{ for } R_t \leq R \leq R_x \quad (4)$$

and

$$\Phi(R) = \frac{(R_t/R)^\beta - (R_t/R_x)^\beta}{1 - (R_t/R_x)^\beta}, \text{ for } R_t \leq R \leq R_x. \quad (5)$$

The observed roll-off for an empirically-determined power-law size distribution may be due to either undersampling or the physical controls on the size of the largest event (Burroughs and Tebbens, 2001). Various statistical techniques developed for earthquake observations can also be applied to constrain the tail of the tsunami size distribution as discussed in Section 4 below.

Undersampling of tsunamis in catalogs occurs both through censoring of small events and having a catalog of insufficient duration to capture the rate of large events. For global catalogs prior to the mid-20<sup>th</sup> century, the locations of tide gage stations are sparse in comparison to the locations of earthquakes that generate measurable small tsunamis (spatial or geographic censoring). In addition, many routine catalogs of tide gage stations sampled water level on an hourly basis until the installation of the 6-minute sample period Analog-to-Digital-Recording (ADR) tide gages starting in the late 1960s and early 1970s (temporal or instrumental censoring). Because the average tsunami period is typically smaller than 1 hour and tsunami amplitudes less than ~10–20 cm are difficult to identify in the presence of ambient noise, smaller events (in amplitude and wavelength) tend to be temporally censored at tide gage stations. Archived analog records of tsunami events can be digitized at a much smaller sampling rate for future probability studies. Finally, in many locations, the tsunami catalog covers only 100–300 years, which is insufficient to accurately determine the rate of occurrence for the largest tsunamis.

To demonstrate the effects of censoring and catalog completeness on empirical power-law frequency-size distributions, we compare the 275-year tsunami catalog at Acapulco, Mexico with a computationally derived frequency-size distribution described by Geist and Parsons (2006). The tsunami catalog consists of both eye-witness observations of runup height and tide-gage measurements starting in 1950. While the entire catalog includes large runup events prior to the installation of the tide gage station that match the computational curve, censoring is evident in the divergence of the two curves for small event sizes (Fig. 4.2a). Using the tide-gage sub-catalog only, we observe a good correspondence for the small events, but incomplete data to constrain the empirical curve for large events (Fig. 4.2b). The roll-off in the computational curve is caused by a physical limitation of earthquake sizes along the offshore subduction zone (Geist and Parsons, 2006).

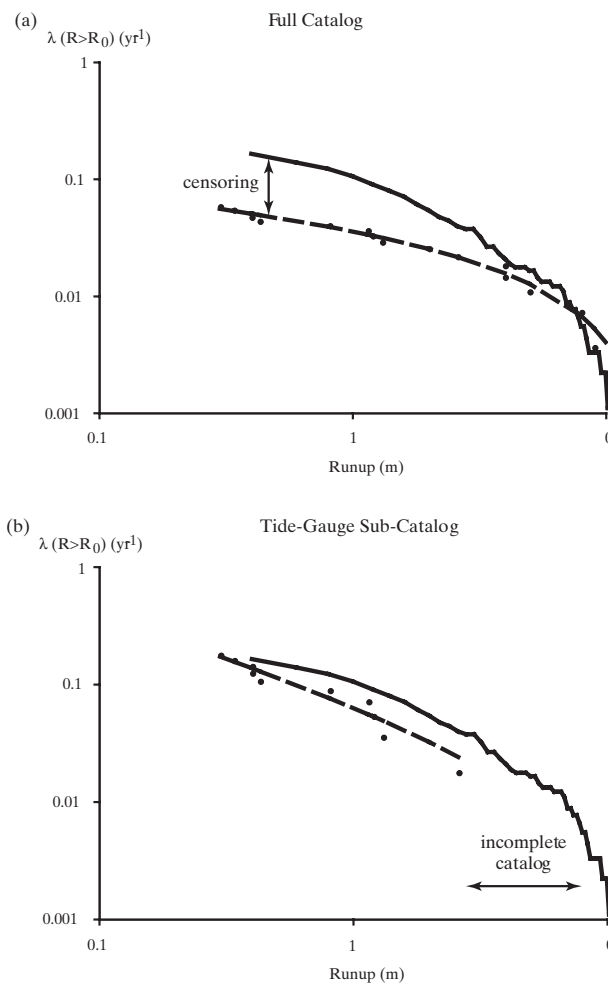


Fig. 4.2 – Observations (solid circles) and best-fit empirical curve (dashed line) representing frequency-size distribution for local tsunamis at Acapulco, Mexico. Computationally-derived distribution (solid line) is shown for comparison. (a) Empirical curve from merged catalog including eye-witness observations and tide-gage measurements (1732–2006). (b) Empirical curve from tide-gage sub-catalog (1950–2006). Modified from Geist and Parsons (2006).

The Acapulco tsunami catalog is an example of a break in an empirical power-law relationship to the left is caused by instrumental censoring (insufficient sampling rate or dynamic range). The completeness threshold for tsunami amplitudes recorded by tide gages as represented in standard tsunami catalogs is approximately 0.1 m. Properly processed, digital tide gages can record tsunamis  $< 0.1$  m. However, many small events are not retained in a permanent archive. Modern deep-sea pressure-sensors that can record micro-tsunamis (Hino et al., 2001; Hirata et al., 2003) will help obviate censoring of small events in the future. In contrast, for a tsunami catalog of sufficient duration that depends on the rate of tsunami activity, a roll-off in an empirical power-law relationship to the right may be an indication of physical limitations to event size (Burroughs and Tebbens, 2001; 2005).

### Distribution of Inter-Event Times

Because sources of tsunamis are generally uncorrelated, tsunami inter-event times can be assumed to be independent, identically distributed (iid) random variables such that the number of events in a particular time increment is independent of the number of events in any other increment. The occurrence of tsunamis under this assumption would accordingly be that of a Poisson process. The probability that  $n$  events will occur within a particular time  $t$  is given by the Poisson distribution:

$$P_n(t) = \frac{(\lambda t)^n e^{-\lambda t}}{n!} \quad (6)$$

where  $\lambda$  is the intensity or rate parameter. We consider here only homogeneous or stationary Poisson processes in which  $\lambda \neq f(t)$ . (An example of a non-stationary Poisson process is the arrival times of earthquakes in an aftershock sequence following a main shock that is discussed below.) The single rate parameter  $\lambda$  at a given location is derived from the aggregation of many sources each with a different source rate parameter as explained in Section 3. The cumulative distribution function (cdf) for  $n$  or more events occurring in time  $t$ , or equivalently, for the  $n$ th event time less than  $t$ , is given by

$$F_{N(t) \geq n}(t) = F_{T_n \leq t}(t) = 1 - \sum_{j=0}^{n-1} \frac{(\lambda t)^j e^{-\lambda t}}{j!}. \quad (7)$$

In hazard analysis, the commonly used special case is of one or more events occurring in time  $t$  resulting in the cdf

$$F_{N(t) \geq 1}(t) = 1 - e^{-\lambda t}. \quad (8)$$

The pdf of event times  $T_n$  can be derived from equation (7) (Kempthorne and Folks, 1971), resulting in the Erlang distribution:

$$f_{T_n}(t) = \frac{\lambda(\lambda t)^{n-1}}{(n-1)!} e^{-\lambda t} \quad (9)$$

The pdf of the first event time  $T_1 = \tau$ , otherwise known as the inter-event or first waiting time, for a Poisson process is an exponential distribution:

$$f(\tau) = \lambda e^{-\lambda\tau}, \quad \text{for } \tau > 0. \quad (10)$$

Empirical estimates of tsunami inter-event times determined by Geist and Parsons (in press) indicate a more complex distribution than would be expected from a stationary Poisson process, but similar to what is observed for earthquake inter-event time distributions. As with empirically derived frequency-size distributions, it is necessary to have a large catalog of events, especially for small amplitude tsunamis that will dominate the left-hand side of the inter-event time distribution. We use, as an example, a global compilation of tide gage tsunami measurements from the National Geophysical Data Center (NGDC) based on a number of original catalogs ([http://www.ngdc.noaa.gov/seg/hazard/tsu\\_db.shtml](http://www.ngdc.noaa.gov/seg/hazard/tsu_db.shtml)). In this case, the event time is defined as the origin time for the tsunami source. An examination of the cumulative number of tsunamis since the start of the 20<sup>th</sup> century indicates that the rate of reported events gradually becomes constant soon after the pivotal 1946 Aleutian tsunami (Fig. 4.3). This time approximately coincides with a sharp increase in the number of sea-level recording station around the world (Caldwell and Merrifield, 2006). With this in mind, we therefore use the portion of the NGDC catalog from 1952–2006. Maximum runup and inter-event time series for the 20<sup>th</sup> century catalog are shown in Fig. 4.4.

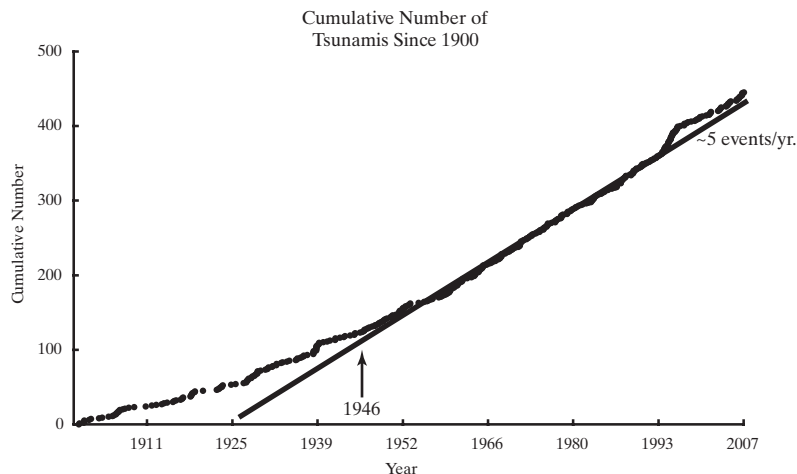


Fig. 4.3 – Cumulative number of tsunamis in the global catalog since 1900.

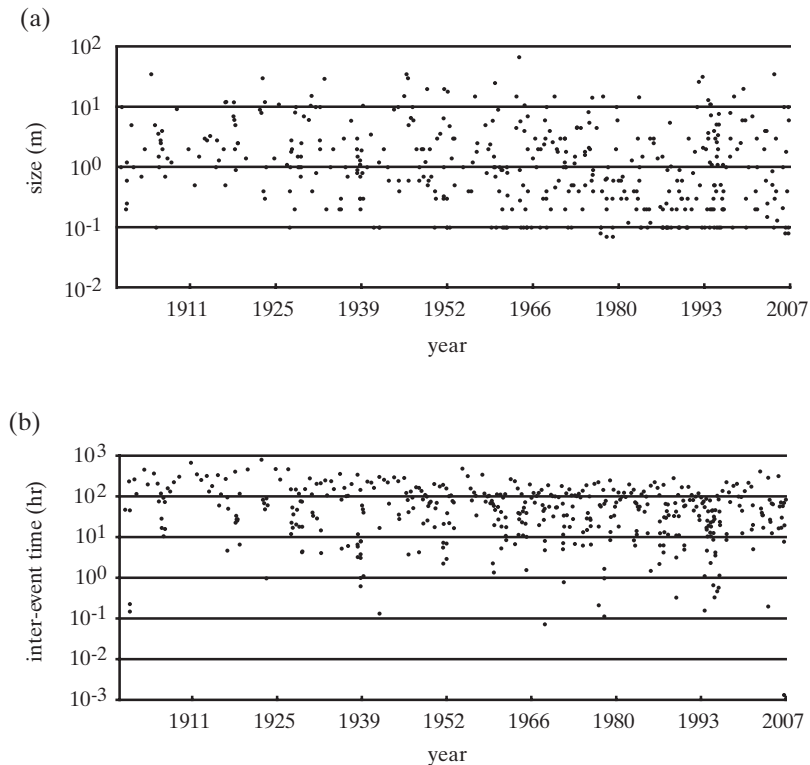


Fig. 4.4 – Time series of global tsunami catalog showing from 1900–2007 showing (a) size of events recorded as run-up heights and (b) inter-event time. Event times are defined as the origin time of the tsunami source.

To determine the empirical pdf, inter-event times were calculated and binned by Geist and Parsons (in press) according to  $c^i$   $i = 1, 2, 3 \dots$ , where the binning constant  $c$  was chosen such that the range of inter-event times encompassed as many bins with non-zero entries as possible (Corral, 2005a). The results of the empirical analysis are shown in Fig. 4.5 in comparison with an exponential inter-event time pdf (equation 10). Here, the rate parameter  $\lambda = N_{cat} / T_{cat}$  is determined from the number of events ( $N_{cat}$ ) over the duration of the catalog ( $T_{cat}$ ) (including the open interval since the last event). From the global catalog, the mean rate is one measured tsunami every 1600 hours, or approximately 5 tsunamis per year. If the frequency-size distribution is also known and can be approximated by a power-law distribution, then the rate parameter is simply  $10^{\alpha_t}$ , where  $\alpha_t$  is relative to the completeness threshold of the tsunami inter-event time catalog (equation 1) (cf., Kagan, 2002a; Ward, 2002).

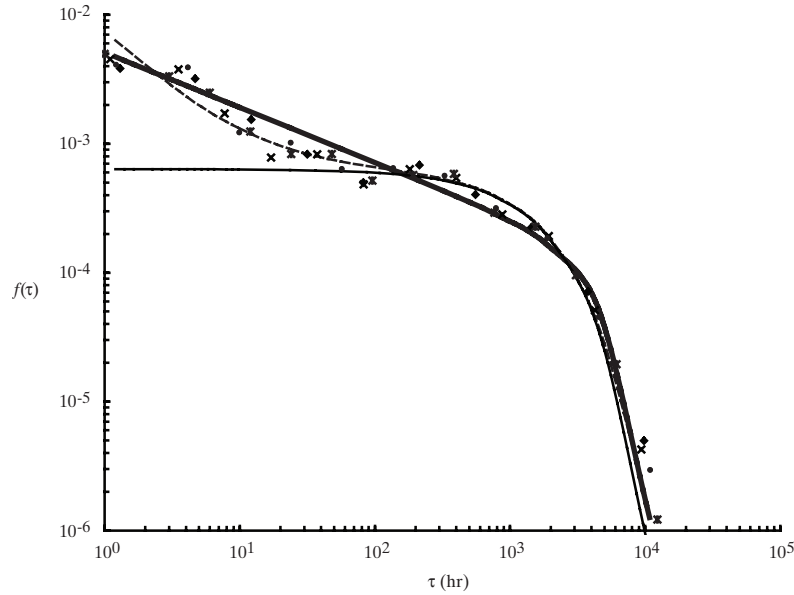


Fig. 4.5 – Empirical pdf for global tsunami source inter-event times using different binning parameters ( $c = 2.0, 2.2, 2.4, 2.6$  hrs.; star, x, circle, diamond, respectively). Theoretical inter-event time distributions also shown for an exponential distribution (light solid line), gamma distribution where  $\gamma = 0.6$  (heavy solid line), and Omori-type aftershock distribution where  $T_a = 9.6$  hrs. (dashed line).

The discrepancy between the empirical and Poisson distribution shown in Fig. 4.5 can be investigated by considering a universal scaling law and an aftershock decay law for earthquake inter-event times. In general, the inter-event pdf is described by the functional form:

$$f(\tau) = \lambda g(\lambda\tau). \quad (11)$$

The universal scaling law proposed by Corral (2004; 2005a) indicates that  $g(\theta)$ , where  $\theta = \lambda\tau$  is the dimensionless inter-event time, can be expressed as a generalized gamma distribution that captures many stationary and non-stationary aspects of observed seismicity:

$$g(\theta) = \frac{C|\delta|}{a\Gamma(\gamma/\delta)} \left(\frac{a}{\theta}\right)^{1-\gamma} e^{-(\theta/a)^\delta}, \quad (12)$$

where  $\Gamma$  is the complete gamma function,  $C$  and  $a$  are normalization and scale constants, respectively, and  $\lambda$  and  $\delta$  are shape parameters. This distribution spans a range of temporal characteristics where  $\gamma = \delta = 1$  is the exponential distribution

(equation 10). The information gain ( $G$ ) of the standard gamma distribution over a Poisson process with rate parameter  $\lambda$  is given by

$$G = \lambda \left[ 1 - \log \lambda + \int_0^{\infty} f(\tau) \log f(\tau) d\tau \right] \quad (13)$$

(Daley and Vere-Jones, 2004; Harte and Vere-Jones, 2005). The information gain is highest for clustering ( $\gamma < 1$ ), but is also significant for  $\gamma > 1$  (i.e., that of a quasi-periodic process) (Harte and Vere-Jones, 2005).

When aftershocks are removed from an earthquake catalog, as in the case of southern California seismicity ( $M \leq 2.5$ ) analyzed by Corral (2005b),  $\gamma \approx 0.7$  indicating that seismicity exhibits weak, longer-term correlations. The physical mechanism of this long-term correlation, which can extend outside the classic aftershock zone, is likely triggering of secondary earthquake from either changes in static stress after each earthquake or dynamic effects from the passage of seismic waves (Parsons, 2002). This distribution also corresponds to world-wide seismicity ( $M \geq 5$ ), suggesting a universal scaling law for earthquake inter-event times, though  $\gamma$  may vary depending on the presence of nonstationary aftershock sequences (Bak et al., 2002; Corral, 2004; Davidsen and Goltz, 2004; Altmann and Kantz, 2005; Molchan, 2005).

Alternatively, an aftershock decay distribution can be used to fit the observed inter-event pdf. This is based on a simplified version of Omori's law. In this case, we fit the observed tsunami inter-event times with an exponential distribution modified with a short-term Omori-law component as

$$f(\tau) = C\lambda \left( e^{-\lambda\tau} + \frac{T_a}{\tau} \right), \quad (14)$$

where  $T_a$  is an aftershock duration time constant. The best-fit gamma and aftershock-decay distribution for the NGDC tsunami compilation are determined by  $\chi^2$ -minimization. This results in estimates of  $\gamma = 0.6$  and  $T_a = 9.6$  hrs. (Fig. 4.5). Other methods of probability model fitting are discussed by Vere-Jones and Ogata (2003). In addition, the Kullback-Leibler, Kolmogorov-Smirnov, and Anderson-Darling statistics can be used to provide an estimate of the goodness of fit (Conover, 1971; Finkelstein and Schafer, 1971; Stephens, 1974; Kotz and Nadarajah, 2000; Parsons, 2002; Daley and Vere-Jones, 2004).

Geist and Parsons (in press) demonstrate that a similar analysis can also be performed for tsunami arrivals at a particular location that has a long record of smaller tsunamis: for example, the Hilo, Hawaii tide gage station (Fig. 4.6). In contrast to the global catalog, the event time in this case is the arrival time of the tsunami at Hilo. The tide gage catalog spans a 60-year range from 1946 to 2007; however, it has only been since 1976 that the tide gage records have been systematically sampled every 6 minutes, rather than every hour. (In most cases, undigitized analog records are also available.) The best fit gamma distribution for these

data has a shape parameter  $\gamma=0.8$ , and a value of  $T_a=1.2$  days for the tsunami aftershock-decay distribution. An examination of the tsunami record indicates several source doublets (2 earthquakes of similar magnitude that occur close in space and time) in the Kurile and Solomon Islands that both triggered tsunamis recorded in Hilo. There is a significant degree of uncertainty in the Hilo distribution, owing to a less than optimal number of data points ( $N=63$ ) required to establish reliable inter-event time statistics.

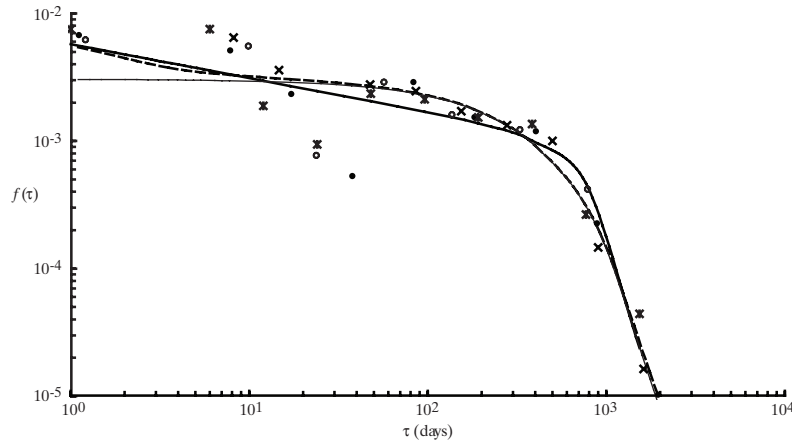


Fig. 4.6 – Empirical pdf for tsunami inter-event times at Hilo, Hawaii using different binning parameters ( $c = 1.8, 2.0, 2.2, 2.4$  days; star, x, filled circle, open circle, respectively). Event times are defined as the absolute arrival time of the tsunami at Hilo. Theoretical inter-event time distributions also shown for an exponential distribution (light solid line), gamma distribution where  $\gamma=0.8$  (solid line), and Omori-type aftershock distribution where  $T_a=1.2$  days (dashed line).

In locations where there are sparse runup data, spatial binning of runup observations and Monte Carlo techniques can be used to estimate the mean rate  $\lambda$  (Geist and Parsons, 2006) (e.g., Fig. 4.7). The single-parameter Poisson distribution should be used for the sparse data case, rather than other distributions such as the gamma distribution above, that require estimation of two or more parameters to define the inter-event distribution. The effect of open intervals (i.e., the time before the first event and the time since the last event) on  $\lambda$  can be estimated by randomly drawing multiple sets of event times from a range of possible  $\lambda$ . By keeping track of which distributions fit the catalog data ( $N$  events over a catalog duration  $T_{cat}$ ) and open intervals, we can estimate the uncertainty in  $\lambda$  (Parsons, in press). The example shown in Fig. 4.7b shows the range of probability for a 30-year exposure time resulting from Monte Carlo uncertainty analysis of the catalog data. A similar analysis is performed for the U.S. West Coast by Geist and Parsons (2006). Further discussion of uncertainty related to empirical probabilities is given in Section 3.2 below in the case of empirical earthquake observations.

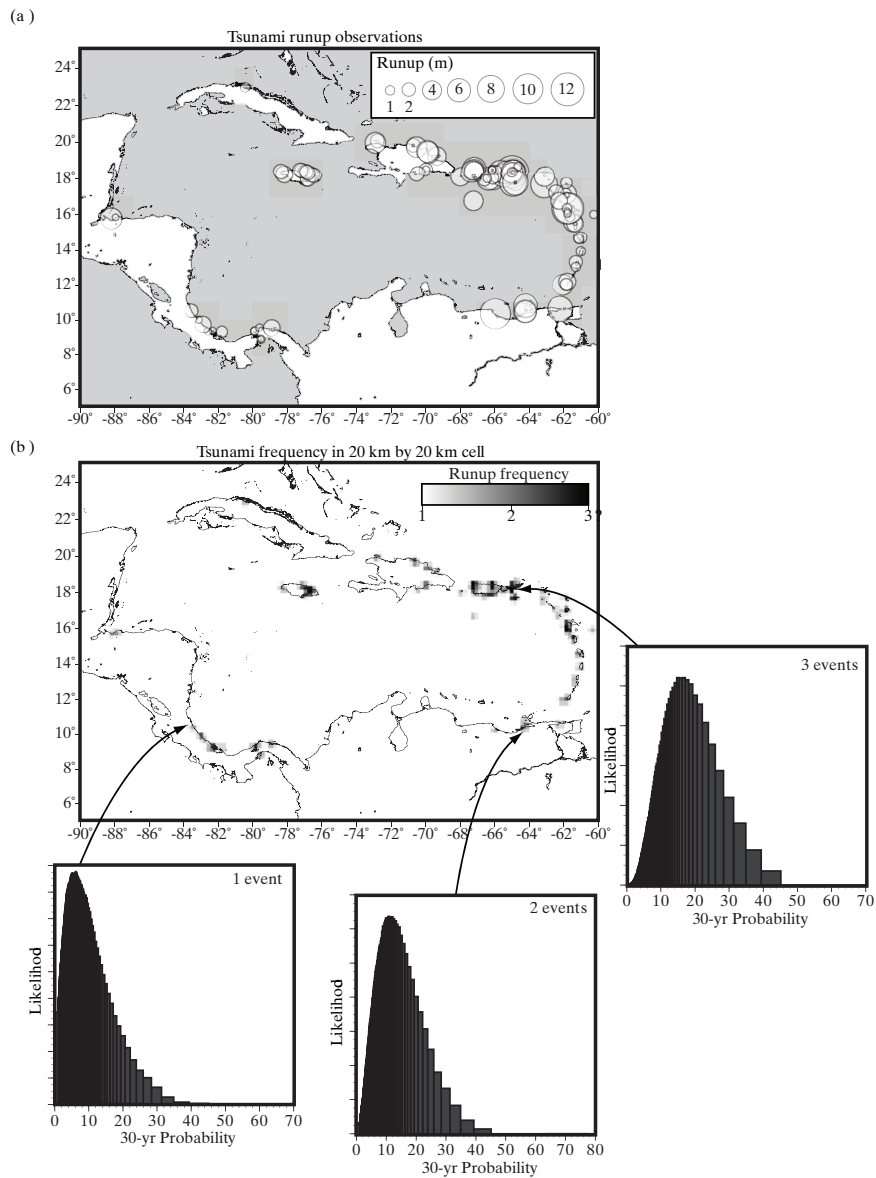


Fig. 4.7 – Regional estimate of tsunami probability in the Caribbean from sparse catalog data. (a) Spatial distribution of tsunami runup observations. Diameter of circle proportional to runup in meters. (b) Frequency of events binned into 20km-by-20km cells. Histograms represent results of Monte Carlo analysis of possible 30-yr. probabilities that fit the catalog data taken from an exponential distribution at 3 representative locations.

### 3. Computational Tsunami Probabilities

In many cases, tsunami probabilities cannot be determined empirically from existing tsunami records. Often this is because there is an insufficient catalog of events for the risk tolerance or design probability of interest. For such a situation, a com-

putational approach to determine tsunami probabilities can be undertaken. In this section, we review the framework of Probabilistic Tsunami Hazard Analysis (PTHA), focusing in particular on how tsunami source probabilities are determined. Even where there is a long catalog of tsunami records, computational PTHA is often a useful technique to test the extent that censoring and catalog completeness affect empirical probabilities as discussed in the previous section and by Geist and Parsons (2006).

### 3.1 Structure of PTHA

PTHA is derived from Probabilistic Seismic Hazard Analysis (PSHA) developed by Cornell (1968) and others and fully described in SSHAC (1997). Like PSHA, PTHA consists of three basic steps: (1) define source parameters, including source probabilities, for all relevant sources; (2) calculate wave heights and other hydrodynamic parameters from a numerical propagation and inundation model for each source; and (3) aggregate the results to determine either the tsunami hazard curve for a particular coastal site or the probabilistic inundation map for a particular coastal region. Lin and Tung (1982) first applied Cornell's (1968) PSHA technique to seismogenic tsunamis, by using simplifying assumptions for the earthquake source and propagation parameters (e.g., constant water depth, etc.). More recent forms of PTHA (e.g., Geist and Parsons, 2006; Thio et al., 2007) involve the use of numerical tsunami propagation models for the second step. Indeed, the processing of this step is one of the primary differences between PTHA and PSHA. As a result of the complexity of wave propagation in the solid earth, standard forms of PSHA are dependent on empirical attenuation relationships (and their attendant uncertainty). PTHA, on the other hand, can take advantage of recent advances in numerical modeling of tsunami propagation and the availability of high-quality bathymetry in most of the world's oceans. The other primary difference is that, in addition to regional and local sources, a comprehensive PTHA must include far-field sources not included as part of PSHA. Depending on the design probabilities and region of interest for PTHA, other sources for tsunamis such as submarine landslides and volcanic sources may also have to be included.

Defining the size parameter linked to source probability is central in PTHA calculations. For earthquakes, this parameter is seismic moment defined as  $M = \mu \bar{D} A$ , where  $\mu$  is the shear modulus or rigidity and  $\bar{D}$  is the average slip over the area  $A$  of the fault that ruptured during the earthquake. The moment magnitude ( $M_w$ ) is related to seismic moment according to  $M_w = \frac{2}{3} [\log(M) - 9.05]$  (Hanks and Kanamori, 1979).

For seismogenic sources, the vertical component of seafloor displacement dominates tsunami generation. The horizontal component provides an additional small effect on tsunami generation in regions with steep bathymetry over the source region (Tanioka and Satake, 1996). Fault rupture is modeled as an elastic dislocation either using uniform slip (termed a Volterra dislocation) or more generally using distributed slip (cf., Geist and Dmowska, 1999). From this description, coseismic displacement can be computed using analytic expressions for a homogeneous earth structure (e.g., Okada, 1985) and numerical techniques for an inhomogeneous structure (e.g., Yoshioka et al., 1989). For dislocation modeling, most parameters such as average slip and rupture area approximately scale with

seismic moment. Other parameters such as fault dip and elastic rock properties are determined from analyses of past earthquakes, controlled-source geophysical surveys, and laboratory tests. For a more complete description of tsunami generation by earthquakes, see Chapter 5 and review papers by Kajiura (1981), Geist (1999), and Satake (2002).

For landslides, the primary size parameter linked to source probability is volume. Recent studies have indicated that submarine landslides may follow a power-law frequency-volume distribution, similar to their counterparts on land (ten Brink et al., 2006a). Unlike earthquakes in which a single parameter, seismic moment, is the principal parameter influencing tsunami generation, landslide tsunami generation is also heavily influenced by landslide speed (or more specifically, time history of landslide movement). During propagation, recent modeling suggests that landslide tsunamis dissipate more quickly than earthquake tsunamis (Gisler et al., 2006). Also unlike earthquakes, there is not a single constitutive relation that describes tsunami generation from landslides. Tsunami generation depends on the type of failure that occurs—e.g., rotational and translational slides, rock falls, lateral spreads, etc. (Varnes, 1978)—which in turn relates to the mechanical properties of the failed material and the bathymetric slope. Examples of different types of landslide tsunami models developed include mudflows (Jiang and Leblond, 1994), translational slides (Ward, 2001), and granular slides (Heinrich et al., 2001). Chapter 6 reviews tsunami generation by landslides in detail.

The second step of PTHA involves computing tsunami wave heights, runup values, and inundation distances at a particular coastal location for each relevant source. In the far-field, seismogenic tsunami amplitudes closely scale with seismic moment (Okal, 1988; Pelayo and Wiens, 1992). Abe (1995) has developed empirical relationships in which wave height at a particular coastal site can be estimated from seismic moment and distance to the earthquake. However, these expressions do not account for the beaming patterns from long ruptures and focusing or defocusing from propagation path effects (Ben-Menahem and Rosenman, 1972; Okal, 1988; Satake, 2002; Geist et al., 2007). In most cases, tsunami propagation is calculated using various forms of the shallow water wave equation and numerical approximates such as finite-difference or finite-element methods. Initial conditions are primarily provided by the vertical displacement from the earthquake or landslide movement. At a coastal location, if near-shore and overland flow are to be computed, non-linear terms of the shallow water equations, bottom friction, and moving boundary conditions must be included. For a review of these methods, please see Chapters 9 and 10 and Shuto (1991).

For the third step in PTHA, the general equation for aggregating probabilities from different sources can be directly adapted from PSHA methodology (e.g., Senior Seismic Hazard Analysis Committee (SSHAC), 1997) as follows:

$$\lambda(R > R_0) = \sum_{\text{source type}=i} v_i \iint P(R > R_0 | \psi_i, r) f(\psi_i) f(r | \psi_i) dr d\psi_i, \quad (15)$$

where  $\lambda(R > R_0)$  is the mean rate of tsunamis at a coastal location with runup greater than  $R_0$ ,  $v_i$  is the mean rate for source type  $i$  (e.g.,  $i=1 \Rightarrow$  earthquakes,  $i=2 \Rightarrow$  landslides, etc.)  $P(R > R_0 | \psi_i, r)$  is the conditional probability that runup

$R$  will exceed a value  $R_0$ , given a distance to the source  $r$  and source parameter(s)  $\psi$ <sup>1</sup>. In other words, the exceedance probability of  $R_0$  depends on the specified values of  $r$  and  $\psi$ . In addition,  $f(\psi_i)$  and  $f(r|\psi_i)$  are pdf's for  $\psi_i$  and  $r$ , respectively. For example, to calculate the mean rate at which a particular runup  $R_0$  is exceeded for earthquakes randomly distributed in space, Abe's (1995) empirical relationships could be used to determine  $P(R > R_0 | M, r)$ ,  $f(\psi_1 = M)$  could be determined from the modified Gutenberg-Richter (G-R) relationship (Kagan, 2002a) and  $f_R(r|M)$  could be dependent on the particular earthquake zonation scheme used (Cornell, 1968; Working Group on California Earthquake Probabilities, 1995; Wesson et al., 1999; Frankel et al., 2002). For earthquakes, a standard zonation scheme such as the Flinn-Engdahl zones can be used (Flinn et al., 1974).

However, in contrast to seismic wave propagation in the solid earth, which is essentially unobstructed, obstruction and scattering from landmasses during tsunami propagation indicates that a distribution based on scalar distance  $f_R(r|m)$  is not practical. In addition, although the approach described by equation (15) may be applicable for asteroid-generated tsunamis randomly distributed throughout the ocean, earthquakes and landslides of tsunamigenic size often occur in distinct source zones. Therefore, an alternative formulation for these sources is

$$\lambda(R > R_0) = \sum_{\text{type}=i} \sum_{\text{zone}=j} \nu_{ij} \int P(R > R_0 | \psi_{ij}) f_{\psi}(\psi_{ij}) d\psi. \quad (16)$$

In this case,  $P(R > R_0 | \psi_{ij})$  is determined for each source type ( $i$ ) and source zone ( $j$ ) from numerical propagation modeling that explicitly includes distance attenuation and propagation path effects, as well as uncertainty in location within the source zone. For source parameters that correlate strongly with a source parameter linked to  $\nu_{ij}$  (e.g., average slip scaling with scalar seismic moment in the earthquake case and runout linked to volume in the landslide case), uncertainty can be included in the  $P(R > R_0 | \psi_{ij})$  term, particularly when the parameters are normally distributed. Details are described in Section 4 on uncertainties. As with empirical tsunami probabilities, the rate term  $\lambda$  is used in the inter-event time distribution to determine the exceedance probability (e.g., equation 8 for the Poisson case). In Sections 3.2 and 3.3 below, we describe how source probability distributions are determined for both earthquakes and landslides.

### 3.2 Source Probabilities: Earthquakes

Because the primary source parameter linked to tsunamigenesis for a particular source zone  $j$  is the scalar seismic moment ( $\psi_{1j} = M_j$ ), we review approaches used to establish frequency-moment relationships for earthquakes. Time-independent and time-dependent probabilities that are described below have frequently been used in the past in relation to earthquake hazards. Examples include probability specifications used in seismic hazard mapping for the U.S. (Wesson et al., 1999; Frankel et al., 2002).

<sup>1</sup> If there is no uncertainty in source location or generation parameters,  $P(R > R_0 | \psi_i, r)$  is simply  $1-H$ , where  $H$  is the Heaviside step function.

### Time Independent Probabilities

Time-independent probabilities assume that earthquakes follow a Poisson process in which the rate term is determined from the G-R power-law relationship. Because earthquakes, like most other natural hazards are size limited, the power-law relationship is modified based on an estimate of maximum moment or *corner moment*. This results in a modified G-R relationship in which the tail of the distribution falls off faster than the power-law exponent ( $\beta$ ). Earthquakes of tsunamigenic magnitude occur near the tail of this distribution where earthquakes catalogs may be incomplete. Therefore, different forms of the frequency-magnitude distribution tail (Fig. 4.8) need to be understood.

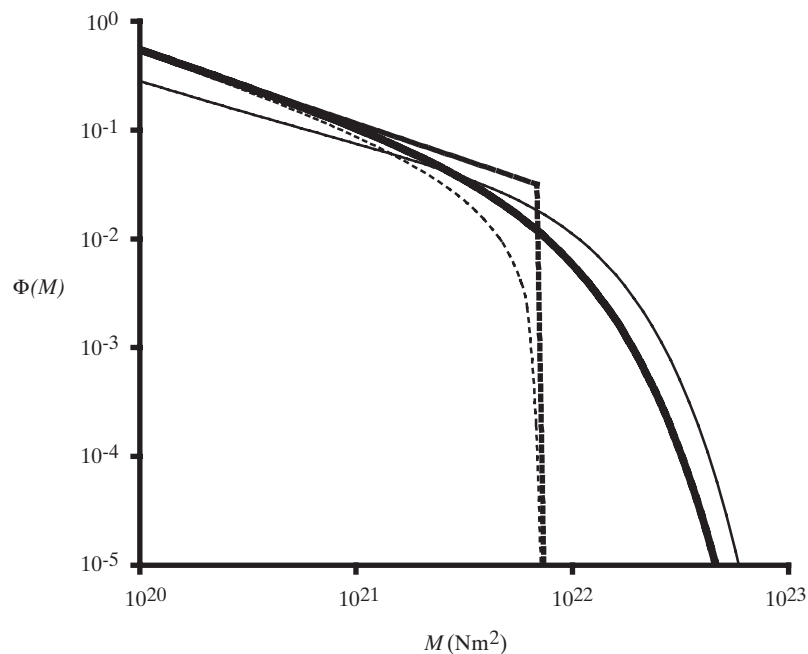


Fig. 4.8 – Different forms of the modified G-R frequency-moment ccdf for earthquakes (Kagan, 2002a). Two pairs of distributions are indicated: characteristic (heavy dashed line) and truncated (light dashed line) distributions have a finite limit. Tapered G-R (heavy solid line) and gamma (light solid line) distributions have a soft taper. For each distribution, the limiting moment and corner moment are identical:  $6.92 \times 10^{21} \text{ Nm}^2$  ( $M_w = 8.5$ ).

In addition to the modified G-R distribution, a different distribution called a characteristic earthquake distribution has been proposed. Because the characteristic earthquake distribution is so widely referred to in the literature, it is important to describe the differences between the two basic distribution types. Characteristic earthquakes are usually defined from the largest recorded earthquake or geometrical differences along a fault zone defining an earthquake segment (Kagan, 1993; Wesnousky, 1994). In the case of tsunamigenic earthquakes, for example, morphological features of the downgoing plate in subduction zone can define segment boundaries and/or coincide with the extent of historic ruptures (McCann et al.,

1979; Nishenko, 1991). The characteristic earthquake distribution considered by Wesnousky (1994) is for the case where there is a gap in earthquake magnitudes (in the discrete form) between the characteristic magnitude  $M_{max}$  and the largest aftershock specified according to Båth's law. The identification of characteristic earthquake distributions is prone to undersampling. Several authors (Howell, 1985; Kagan, 1993; Stein and Newman, 2004) have demonstrated that if a G-R distribution is undersampled it tends toward an apparent characteristic distribution. In addition, physical models of rupture over many earthquake cycles indicate that rupture can appear to follow an characteristic mode for a number of earthquake cycles and then revert back to a G-R mode (Shaw and Rice, 2000; Shaw, 2004). For uniform fault properties, the rupture mode may be persistently characteristic (Ben-Zion, 1996; Lu and Vere-Jones, 2001; Zeng et al., 2005). However, many faults appear to be characterized by a combination of three factors: self-affine complexity caused by material heterogeneity (e.g., Perfettini et al., 2001; Shaw, 2004); static changes in stress on the fault from neighboring earthquakes (e.g., Marsan, 2005; Parsons, 2005; 2006); and the dynamics of earthquakes themselves (e.g., Cochard and Madariaga, 1996; Ben-Zion and Rice, 1997; Shaw and Rice, 2000). This complexity is typically expressed as a modified G-R distribution of earthquake magnitudes.

As summarized by Kagan (2002a), there are four basic forms of the modified G-R distributions: two truncated forms (i.e., hard corner) and two tapered forms (i.e., soft corner) (Fig. 4.8). Kagan (2002a) notes that most driven dissipative systems, such as earthquakes, exhibit a smooth transition toward the extreme value of the distribution defined by a corner moment  $M_c$ . For this reason, tapered distributions have been developed for both the ccdf (tapered G-R distribution with corner moment  $M_{cm}$ )

$$\Phi(M) = \left(\frac{M_t}{M}\right)^\beta \exp\left(\frac{M_t - M}{M_{cm}}\right), \text{ for } M_t \leq M \quad (17)$$

and for the pdf (gamma distribution with corner moment  $M_{cg}$ )

$$\phi(M) = \frac{\beta}{CM} \left(\frac{M_t}{M}\right)^\beta \exp\left(\frac{M_t - M}{M_{cg}}\right), \text{ for } M_t \leq M, \quad (18)$$

where  $C$  is a normalizing coefficient (Kagan, 2002a). (See Kagan 2002a for the pdf and ccdf of the tapered and gamma distributions, respectively.) The parameters that define the earthquake distribution ( $\beta$ ,  $M_c$ ) have been estimated for different types of plate boundaries and a number of different seismic zonation schemes using primarily maximum likelihood methods (Kagan, 1997; 1999; 2002a; b; Bird and Kagan, 2004). The commonly used  $b$ -value for earthquakes is based on  $M_w$ , whereas  $\beta$  is based on seismic moment  $M$  such that  $\beta = \frac{2}{3}b$  according to the definition of moment magnitude.

Because large earthquakes are rare, the tails of earthquake distributions are difficult to determine from historical seismicity alone. For this reason, a seismic moment balance argument has previously been used to determine the expected

earthquake distribution. Moment balance requires knowledge of the long-term fault slip rate, seismogenic thickness, and the seismic efficiency or coupling constant. For plate boundary faults, recent global studies yield information on long-term fault slip rate (Bird, 2003; Kreemer et al., 2003). The rate parameter ( $\nu_{ij}$ , cf., equation 16) for seismic moments greater than or equal to  $M_0$  can be linked to the parameters to the modified G-R distributions expressed in equations 17 and 18 as follows (Kagan, 2002b):

$$\nu(M \geq M_0) = \xi_m^{-1} \left[ \frac{1-\beta}{\Gamma(2-\beta)} \right] \frac{\dot{M}_s}{M_0^\beta M_{cm}^{1-\beta}} \quad (19)$$

and

$$\nu(M \geq M_0) = \xi_g^{-1} \left[ \frac{1-\beta}{\Gamma(2-\beta)} \right] \frac{\dot{M}_s}{\beta M_0^\beta M_{cg}^{1-\beta}}, \quad (20)$$

respectively, where  $\xi_m$  and  $\xi_g$  are correction coefficients given in Kagan (2002b). Ward (1994) develops a similar expression for the truncated G-R distribution. In equations 19 and 20,  $\dot{M}_s$  is the rate of seismic moment release that ideally can be determined from earthquake catalogs. Using the seismic moment balance approach, however, the maximum seismic moment rate at seismogenic depths can be constrained by the fault slip rate if one assumes an efficiency or coupling constant  $\chi = 1$  (i.e., no aseismic slip at depths where earthquakes typically occur):

$$\dot{M}_s = \mu L H_s \dot{s}_{tect}, \quad (21)$$

where  $\mu$  is the shear modulus,  $L$  fault length,  $H_s$  effective seismogenic thickness (which includes the parameter  $\chi$ ), and  $\dot{s}_{tect}$  the long-term (tectonic) fault-slip rate (Ward, 1994).

Note that the rate of large earthquakes along subduction zones is primarily linked to relative convergence rates and that factors such as age of subducted lithosphere, time since the last event, etc. do not strongly correlate with seismic activity (Bird and Kagan, 2004). The seismic coupling constant ( $\chi$ ) that appears in the definition of  $H_s$  above remains an elusive parameter. However, statistical analysis suggests that there may be little variation among plate boundary faults, such that  $\chi \geq 0.5$  in most cases (Kagan, 2002b) and that  $\chi \rightarrow 1$  for shallow faults (Kagan, 1999). A value of  $\chi = 1$  provides an upper limit of activity rate for the seismic moment-balanced size distribution of earthquakes.

### Time-Dependent Probabilities

In the past, large tsunamigenic earthquakes along subduction zones have considered to follow a quasiperiodic process specifically conditioned on the preceding event, in which the probability of the next earthquake is dependent on the time since the last earthquake. Such time-dependent probabilities are most often applied to characteristic earthquakes as defined above. Three basic forms are commonly used for earthquake probabilities in which the occurrence of one or more

earthquakes in the time interval  $T$  is conditional upon the time since the last earthquake  $\tau$ :  $F_{N(T) \geq 1}(T | \tau)$  (Utsu, 1984). The corresponding pdf's for the inter-event time are given for the (1) Weibull distribution (e.g., Rikitake, 1999)

$$f(\tau) = \alpha v(\tau)^{\alpha-1} \exp(-v\tau^\alpha) \quad (22)$$

(2) Log-normal distribution (e.g., Nishenko and Buland, 1987)

$$f(\tau) = \frac{1}{\alpha\tau\sqrt{2\pi}} \exp\left[-\frac{(\ln(v\tau))^2}{2\alpha^2}\right] \quad (23)$$

and (3) Brownian-Passage time (BPT) distribution (Matthews et al., 2002)

$$f(\tau) = \left(\frac{1}{2\pi v\alpha^2\tau^3}\right)^{1/2} \exp\left[-\frac{v(\tau-1/v)^2}{2\alpha^2\tau}\right]. \quad (24)$$

All three forms are similar in that three parameters are needed to define the distributions: the mean inter-event time ( $1/v$ ) as in the Poisson distribution (equation 8), the time since the last earthquake ( $\tau$ ), and the shape or aperiodicity parameter  $\alpha$ . (In equations 23 and 24,  $\alpha$  is similar to standard deviation and coefficient of variation, respectively; although strictly speaking these terms refer to sample statistics.) Parameter estimation for the Weibull and log-normal distributions using the method of moments and maximum likelihood are given by Utsu (1984).

As noted by Matthews et al. (2002), there are important differences in the hazard rate function  $h(\tau)$  among these distributions:

$$h(\tau) \equiv f(\tau)/[1-F(\tau)], \quad (25)$$

where  $F(\tau)$  is the cdf corresponding to  $f(\tau)$ . The hazard rate function can also be thought of as the instantaneous failure rate or the failure probability conditional upon surviving up to point  $\tau$ . For equivalent distribution parameters, the BPT distribution is characterized by a nearly constant hazard rate at long waiting times, whereas the hazard rate decreases for the log-normal distribution and increases for the Weibull distribution for long waiting times. Matthews et al. (2002) indicates that the gamma distribution for a quasiperiodic process is characterized by an increasing hazard rate (though not as sharply as the Weibull distribution) for  $\gamma > 1$  (cf., equation 12). As shown in Fig. 4.9, the gamma distribution discussed in connection with tsunami inter-event times in Section 2 characterized by  $\gamma < 1$  is, in contrast, associated with decreasing hazard rate function for short waiting times and nearly constant hazard rate at long waiting times (Corral, 2005c). Thus at  $\gamma = 1$ , the change in exponent represents a fundamental difference between a quasiperiodic process  $\gamma > 1$  and a clustering process  $\gamma < 1$  (Utsu, 1984), and a corresponding change from a increasing hazard rate to a decreasing hazard rate, respectively.

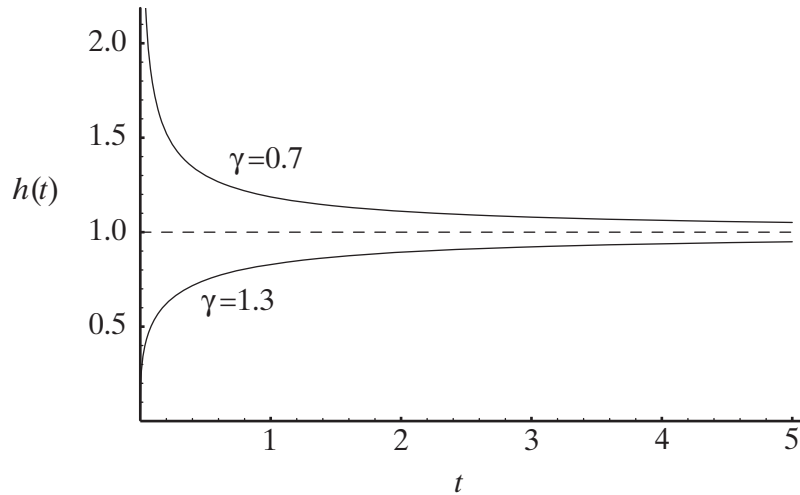


Fig. 4.9 – Hazard rate as a function of non-dimensional time  $h(t)$  for two gamma distributions with different shape parameters: increasing hazard rate ( $\gamma > 1$ ) with time associated with quasiperiodic models (e.g., Ogata, 1999); decreasing hazard rate ( $\gamma < 1$ ) associated with temporal clustering of events (e.g., Corral, 2004). Constant hazard rate for exponential distribution (dashed line) shown for comparison.

For multiple time-dependent tsunamigenic earthquakes, a different method of aggregation must be used instead of equation 16. The probability of a tsunami at a particular coastal location generated by the  $j$ th characteristic earthquake and within an exposure time  $T$  is given by  $P(R \geq R_0 | \psi_{i=1,j}, T)$ . The parameter set  $\psi_{i=1,j}$  includes the parameters that define the time-dependent probability distribution ( $t_0, \nu, \alpha$ ) as well as the source parameters needed to compute tsunami generation. The aggregate tsunami probability of  $N$  characteristic earthquakes  $P(R \geq R_0 | T)$  is given by Rikitake and Aida (1988):

$$P(R \geq R_0 | T) = 1 - \prod_{j=1}^N [1 - P(R \geq R_0 | \psi_{i=1,j}, T)]. \quad (26)$$

For subduction zones, McCann et al. (1979) and Nishenko (1991) presented seismic hazard maps based on characteristic earthquakes (described previously) using the log-normal event distribution (equation 23) that could be used in the aggregation equation (26). The seismic hazard was expressed as the probability of occurrence during exposure times of 5, 10, and 20 years for a characteristic earthquake occurring along a segment defined primarily by historic earthquake rupture lengths. This is generally known as the *seismic gap hypothesis*. The Nishenko/McCann time-dependent probabilities have been evaluated using different statistical tests in a number of papers (Lomnitz and Nava, 1983; Kagan and Jackson, 1991; 1995; Rong et al., 2003). The general conclusion of these papers is that in comparison to actual earthquake occurrence, the time-dependent probability estimates in most cases did not perform as well as the probabilities calculated from a time-independent, Poisson null or reference model. Along fault zones where there

is a significant difference between the seismic moment rate ( $\dot{M}_s$ ) determined from an earthquake catalog and that determined from tectonic parameters (equation 21), the deficit may be resolved by future large earthquake(s), depending on the uncertainty in the coupling constant  $\chi$ . However, according to the statistical tests, no segment is more or less likely to fail based on the time since the last event (Bird and Kagan, 2004).

The other problematic issue related to time-dependent probabilities is the estimation of the three parameters that define the distributions ( $\tau$  can be uncertain if the preceding earthquake is prehistoric.) The assumption of a generic aperiodicity parameter ( $\alpha = 0.21$ ) for all faults, termed the Nishenko-Buland hypothesis, is shown not to be valid by Savage (1991). To determine the mean inter-event time in the absence of numerous paleoseismic records of past events, a time-predictable model (Shimazaki and Nakata, 1980) is often assumed. This is termed the *direct method* for determining earthquake recurrence in which the mean slip for an earthquake segment and the long-term slip rate can be used to determine mean inter-event time. Each of these parameters, however, has large uncertainties. Savage (1991) demonstrates that the corresponding uncertainty in the probability distribution can be so large such that the probability estimate is not very different from an informationless system. Recent observational studies indicate that neither the time-predictable nor slip-predictable models are valid starting assumptions for determining inter-event time or magnitude, respectively (Murray and Segall, 2002; Weldon et al., 2004; Weldon et al., 2005).

For faults where there are many paleoseismically-identified event horizons, it may be possible to avoid the direct method and time-predictable assumptions indicated above. For tsunamigenic earthquakes generated along subduction zones where there is no near-surface exposure of the fault, evidence of coastal subsidence in the geologic record is used to identify pre-historic earthquakes (see Chapter 3 and Atwater et al., 2004). However, in these cases a purely empirical determination of mean inter-event time and aperiodicity remains problematic. This is the classic case of how probability varies as a function of the number of Bernoulli trials—that is, the use of additional observations to improve a prior probability distribution through Bayes' theorem. For earthquake observations, Savage (1994) indicates that the uncertainty in probability decreases slowly with the number of observed paleoseismic events. Suppose there are  $m$  out of  $n$  recorded inter-event times less than exposure time  $T$ , then the probability density  $P(p|m,n)$  that the next event will occur within time  $T$  since the most recent earthquake follows the distribution:

$$P(p|m,n) = \left[ \frac{(n+1)!}{m!(n-m)!} \right] p^m (1-p)^{n-m}, \quad (27)$$

with expected value

$$\langle p \rangle = \frac{m+1}{n+2} \quad (28)$$

and variance

$$\sigma^2 = \frac{\langle p \rangle (1 - \langle p \rangle)}{n + 3}. \quad (29)$$

Without using assumptions about the underlying event distribution, determination of empirical probabilities using this method is based on a uniform distribution in the absence of any observations, also known as the principle of indifference. For a summary of arguments and interpretations of this technique, the reader is referred to Howson and Urbach (1993) and Jaynes (2003).

As an example, we consider the uncertainty in the probability of future tsunamigenic earthquakes along the Cascadia subduction zone, using the identified horizons indicated top left corner of Fig. 4.10a. Measuring inter-event times from the center of the age range for each horizon, the mean inter-event time is 517 yrs, with  $m=4$  out of  $n=6$  inter-event times being less than this value. The expected probability of having another earthquake within 517 years after the last event (1700) is therefore 0.62. However, the 95% confidence interval for this estimate is 0.34-0.87, indicating a high degree of uncertainty. For 10 or fewer paleoseismic horizons, Savage (1994) indicates that the probability cannot be determined better than  $\pm 0.2$ .

Next, we consider uncertainty associated with age-dating of each event horizon that results in a complex probability distribution of for each event (Bronk Ramsey, 1998; Ogata, 1999). In light of this and the open intervals on either end of a paleoseismic sequence (i.e., before the earliest identified event and after the last event) (Davis et al., 1989), Ogata (1999) estimates the uncertainty in the time-dependent distribution parameters ( $\alpha$  and  $\nu$ ). Ogata (1999) assumes a uniform pdf for the possible age of a given paleoseismic horizon, and proposes an inverse probability (Bayesian) method to improve these estimates. Alternatively, Parsons (2005) uses a Monte Carlo method to determine the range of possible values of  $\alpha$  and  $\nu$  for a given paleoseismic sequence. An example of the uncertainty in probability for the events described in the above example using the BPT distribution (equation 24) is shown in Fig. 4.10. In this case, the results from Monte Carlo analysis indicate that  $F_{N(\tau) \geq 1}(T = 30 \text{ yr.}, t_0 = 1700)$  for a time window starting in 2005 ranges between 0.01 and 0.15 (Fig. 4.10b). The conditional probability for an exposure time window that does not begin with the preceding event is given by (Parsons, 2005)

$$F_{N(\tau) \geq 1}(t_0 < \tau \leq t_0 + T) = \int_{t_0}^{t_0+T} f(t) dt. \quad (30)$$

Plots such as shown in Fig. 4.10 are useful for determining how well the paleoseismic data constrain a particular probability distribution. In general, such analysis shows that while a quasiperiodic model of earthquake recurrence is an intuitive representation for an individual fault, in practice it is often difficult to determine the parameters of a particular distribution for subduction zone earthquakes with any degree of confidence.

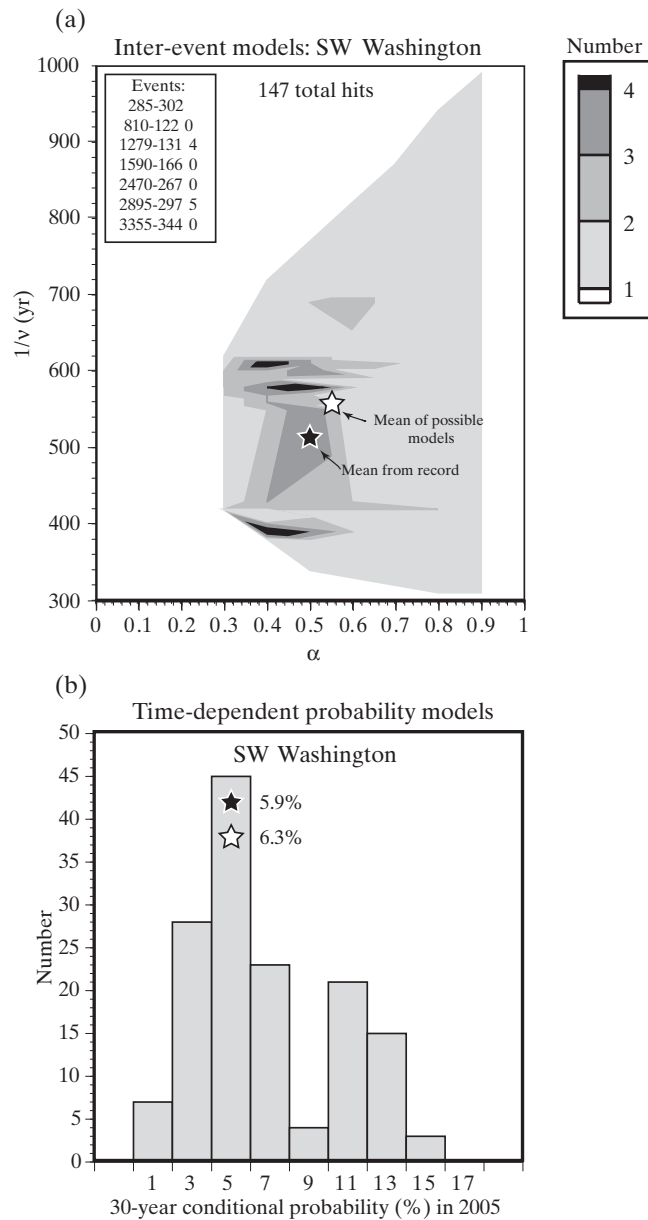


Fig. 4.10 – Results of Monte Carlo simulation in which the successful combinations of parameters  $v$  and  $\alpha$  for the BPT distribution fit the observed paleoseismic record of Cascadia subduction zone earthquakes. (a) number of successful hits for the two distribution parameters. (Mean inter-event time represented by  $1/v$ .) (b) resulting histogram of 30-year conditional probabilities for the distributions that fit the data.

Another particular type of time-dependent probability is clustering of earthquakes in time, caused by foreshocks, aftershocks, and triggering of earthquakes outside the classic aftershock zone through coseismic changes in the static-stress field and through dynamic triggering. In addition to the gamma distribution pro-

posed by Corral (2004) discussed earlier, Kagan and Jackson (2000) model this as a short-term forecasting problem using a negative binomial distribution. Whereas foreshocks are rare, aftershocks are a common phenomena in which the rate of occurrence  $v$  is described by Omori's law:

$$v = c/(p+t)^n, \quad (31)$$

where  $c$ ,  $p$ , and  $n$  are constants and  $t$  is time since the main shock (Parsons, 2002). In addition, changes in the loading stress on a fault from the occurrence of a nearby large earthquake(s), termed the Coulomb failure stress, can significantly affect the short term probabilities (Parsons, 2004; 2005; 2006). Postseismic viscous relaxation of the lithosphere gradually decreases this probability effect over time (Michael, 2005). For tsunami applications, Geist and Parsons (2005) demonstrate that in some cases, large strike-slip earthquakes may trigger tsunamigenic dip-slip aftershocks within days after the mainshock.

### 3.3 Source Probabilities: Landslides

The primary source parameter linked to tsunamigenesis for landslides is volume ( $\psi_{2,j} = V_j$ ); however, landslide speed is also an important controlling variable linked to tsunami generation efficiency. Below we discuss recent work to define landslide volume distributions and how uncertainty in landslide speed can be included in PTHA calculations. In general, landslide source probabilities are particularly difficult to determine, as a result of the lack of age dates for most of the world's submarine slides. In addition, it is difficult to determine a landslide-equivalent quantity such as long-term fault slip rate to estimate the overall activity of landslide occurrence along a particular margin. Nonetheless, recent research suggests the existence of a power-law size distribution for landslides (equivalent to the standard G-R relationship for earthquakes) in specific areas. Also, some geologic analysis has been conducted that may lead to frequency-size distributions and other parameters needed to determine probabilities for landslide tsunami sources.

ten Brink et al. (2006a) demonstrated that the distribution of submarine landslides north of Puerto Rico follow a power-law relationship with an exponent ( $\beta$ ) similar to that found for rock falls onland (Stark and Hovius, 2001; Guzzetti et al., 2002; Dussauge et al., 2003; Malamud et al., 2004). Including small landslide sizes on land, the most descriptive distribution for the entire range of sizes is in fact the double Pareto distribution described by Stark and Hovius (2001). An empirical analysis of the submarine Storegga landslide complex initially suggested that the number-size distribution follows a logarithmic distribution (Issler et al., 2005). However, when the largest distinct landslides are included, ten Brink et al. (2006) confirms that the distribution follows a power-law relationship. Unlike earthquakes, the value of  $\beta$  varies significantly for landslides (e.g., comparison of the Storegga and Puerto Rico landslide regions:  $\beta = 0.44$  and  $0.64$ , respectively), indicating that the failure process significantly affects scaling (Malamud et al., 2004).

In examining the physical mechanisms that give rise to this power law relationship, Hergarten and Neugebauer (1998) indicate that a state variable in addition to slope gradient is necessary for landslides to follow a power-law size distribution.

This is generally termed a time-weakening effect (Densmore et al., 1998; Hergarten, 2003) and is similar to a quasiperiodic process in that the probability of failure increases with waiting time after the last event at a particular source location. Examples of time-weakening effects include strain softening, creep, and redistribution of pore pressures following, for example, earthquakes (Biscontin et al., 2004; Biscontin and Pestana, 2006). Dugan and Flemings (2000) also describe a process of lateral pressure equilibration over time for submarine fans, with a gradual increase the likelihood for failure.

The power-law exponent  $\beta$  for landslide volumes can be determined from either cumulative distributions or rank-order distributions. For the latter, observations are sorted from largest (rank  $n=1$ ) to smallest (rank  $n=N$ ). An advantage of rank-ordering is that it tends to avoid bias introduced by correlations of statistical fluctuations that can be present in cumulative distributions (Sornette, 2004). As an example, the rank-order distributions of landslides offshore northern Puerto Rico (ten Brink et al., 2006a) are presented in Fig. 4.11. The power-law portion of the distribution given by

$$V_n \propto n^{-1/\beta}, \quad 1 \ll n \leq N \quad (32)$$

where  $n$  is the rank order and  $V_n$  is the volume associated with the  $n$ th rank order (Sornette, 2004). In this case,  $\beta = 0.62 \pm 0.03$  determined from the rank-order distribution is similar to  $\beta = 0.64$  determined from the cumulative statistics of landslide volumes presented by ten Brink et al. (2006a). This is smaller than the exponent found for clay-rich, less cohesive landslides, but similar to that found for sub-aerial rockfalls, indicating the effect that mechanical properties has on landslide statistics (Densmore et al., 1998; Dussauge et al., 2003; ten Brink et al., 2006a)

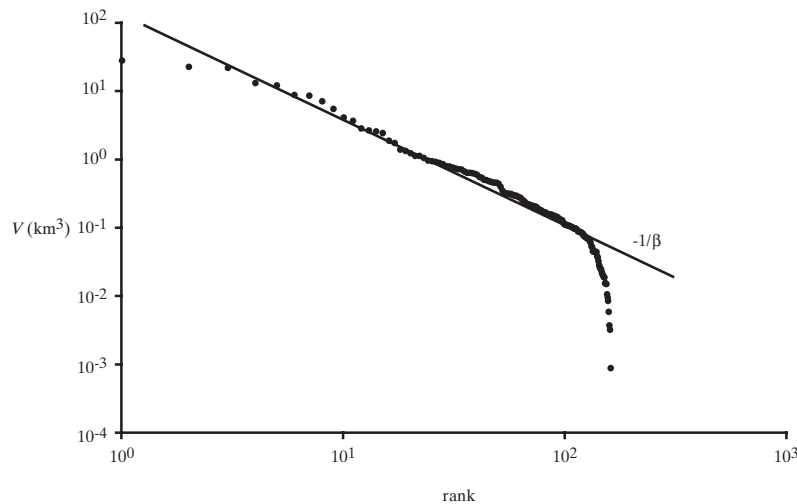


Fig. 4.11 – Rank order distribution of landslide volumes offshore northern Puerto Rico. Power-law exponent ( $\beta=0.62\pm0.03$ ) determined from this distribution is similar to that determined from the cumulative distribution of volumes (ten Brink et al., 2006a).

Even if landslides are assumed to follow a Poisson process, in most locations there is insufficient information with which to determine the rate parameter ( $\nu_{2j}$ , equation 16) or equivalently the activity constant  $\alpha$  in the frequency-size power-law relationship (equation 1). There is some indication from modeling and empirical results that the rate of landslide occurrence is non-stationary, depending on long-term global sea level fluctuations (Hutton and Syvitski, 2004). Determination of both  $\alpha$  and  $\beta$  rely on the correct identification of individual slide events (in terms of the tsunami they generate) and age dating. In the past, low resolution imaging of landslide features led in some cases to the misidentification of individual landslide events. Large complexes and amphitheatres that spanned a considerable geologic age range in geomorphic development were often considered one event. With the advent of high-resolution sea floor imaging techniques such as multibeam bathymetry, it has been easier to identify individual landslide events (Lee, 2005; ten Brink et al., 2006b).

Age-dating of individual events necessitates identification of geologic horizons that span the age of failure. For example, Normark et al. (2004) recognized a debris flow unit in a piston core that appeared to correspond to a part of a large landslide complex, the Palos Verdes debris avalanche near Los Angeles identified using multibeam imagery. By obtaining C-14 ages of microfauna in units above and below the debris flow in the piston core, they were able to estimate the age of the landslide component as 7500 yr. In some locations, multiple failures at the same location are observed using seismic-reflection profiling. For example, for the Goleta landslide complex in Santa Barbara Channel, Fisher et al. (2005) identify 7 different failure events beneath one of the three major lobes. By following acoustic reflectors to the location of a nearby ODP boring, the authors determined that three of the failures occurred in the last 160 ka. Lee et al. (2004) assembled available age-date information for submarine landslides in southern California and estimated that large failures ( $V > 0.5 \text{ km}^3$ ) recur with a time interval in the range of 5,000 to 10,000 years.

Seven large pre-Holocene landslides have occurred at the location of the massive Storegga Slide complex off Norway (Solheim et al., 2005a). These were identified and dated using seismic reflection profiling, borings and core samples. The investigations show that at least one large landslide apparent occurs during every 100 ky, following glacial-interglacial cyclicality, with the most recent occurring 8,150 years ago. Accordingly, investigators have been able to conclude that the slope stability environment at the site of the Storegga complex will take another glacial-interglacial cycle to form a situation that could lead to another major tsunami-generating slide (Solheim et al., 2005b). The site is considered to be safe for development of a large gas field for the foreseeable future. Few other locations worldwide have received the kind of attention directed to southern California and Norwegian submarine landslides so recurrence interval information available for these environments is generally lacking. To identify these sediments requires either coring the debris field multiple times in the hope of collecting cores with sediment and the underlying debris, or conducting high-resolution seismic imaging to direct the coring. Even with these techniques, the age of some landslides may not be dated precisely, because of a very low sedimentation rate or lack of datable material.

If the rate of landslide recurrence can be determined through accurate event identification and age dating, it is still necessary for tsunami computations to determine the time history of landslide failure. As indicated by several authors (e.g., Ward, 2001; Todorovska et al., 2002; Trifunac et al., 2002), tsunami generation efficiency is dependent on landslide speed. Landslide dynamics is a complex field of research, and there are different measurements of landslide speed, the most applicable for the outgoing tsunami being the spreading velocity (Todorovska et al., 2002; Trifunac et al., 2002; 2003). In the near-field, other parameters such as slide shape and submergence relative to slide height are important factors in determining runup (Liu et al., 2005). Some source parameters such as runout may scale with volume and may not be mutually independent. In addition, examination of a global tsunami catalog indicates that most tsunamigenic landslides are associated with earthquakes, much like subaerial landslides in seismically active regions (Keefer, 1994). The origin of the triggering mechanism is thought to be direct loading from the earthquake and changes in the pore pressure from successive seismic loading cycles (Biscontin et al., 2004; Biscontin and Pestana, 2006). For non-seismically triggered landslides, very low tidal excursions is a common triggering mechanism in which the slide loses its hydraulic support and does not dewater rapidly. More research is needed to determine the inter-relationship among landslide source parameters that affect tsunami generation and the mobility of submarine landslides in general (Locat and Lee, 2002; Locat et al., 2004). In the meantime, equation 16 can be used to determine landslide probabilities using characteristic parameters (and their attendant uncertainty) for a given region, such that normally distributed uncertainty is included in the  $P(R > R_0 | \psi_{i,j})$  term.

#### 4. Uncertainties

The determination of uncertainty in the seismic component of the computational PTHA is highly dependent on the underlying assumptions of earthquake physics. For example, if a characteristic, time-dependent rupture model is assumed, there is little uncertainty in the magnitude of the characteristic event, whereas there is large uncertainty in the parameters that define the earthquake recurrence distribution (Savage, 1991; 1992). Similarly, if a slip-predictable model is assumed, then there is little uncertainty in the magnitude of the next event, but large uncertainty in the waiting time of the next event (Shimazaki and Nakata, 1980). Recent research in earthquake physics has indicated that the earthquake rupture process is sufficiently complex over multiple earthquake cycles and considering multiple faults. For the purposes of probabilistic analysis, tsunamigenesis can be considered a stochastic process, with random variables described in the aggregation equations. In this section we will briefly describe the ergodic assumption used in several aspects of PTHA and indicate how epistemic and aleatory uncertainties are incorporated in PTHA. We will also examine the special case of estimating extreme values for tsunami runup.

##### 4.1. The Ergodic Assumption

In estimating certain source parameters or their uncertainty, it is often necessary to assume that the physical process (landslides, earthquakes, etc.) is ergodic.

Although the ergodic theorem originating from statistical physics is complex and multifaceted (Anosov, 2001), one important application of the theory is that the time average of a process ( $x$ ) at a particular geographic point is equal to the average at a particular time ( $t_0$ ) over an ensemble of points  $x_k$  (Beichelt and Fatti, 2002):

$$\lim_{T \rightarrow \infty} \frac{1}{2T} \int_{-T}^T x(t) dt = \lim_{N \rightarrow \infty} \frac{1}{N} \sum_{k=1}^N x_k(t_0) \quad (33)$$

For natural hazards, this allows replacing an estimate of the source or hazard statistics at a particular location where there is limited knowledge throughout time with the statistics of an ensemble of known source or hazard variables over a broad region (or even globally).

An example of where the ergodic assumption is used is estimation of corner moment for a particular fault. Because earthquake catalogs are very limited at large magnitudes for a particular fault zone or fault segment throughout time, it is necessary to analyze the statistics of corner moment for a number of faults around the world, as done by Bird and Kagan (2004). However, Bird and Kagan (2004) note that different types of faults (oceanic transform faults, subduction zones) are separated because of differences in tectonic environment (stress, thermal structure, etc.) (see also Pisarenko and Sornette, 2003). Grouping all subduction zones together, Bird and Kagan (2004) were able to estimate a corner moment magnitude of 9.58. Even with the expanded catalog of subduction zone earthquakes, however, uncertainty is still difficult to estimate. They indicate 95% confidence limits of  $9.58_{-0.46}^?$  (upper confidence limit not found) using a merged 20<sup>th</sup> century earthquake catalog and  $9.58_{-0.46}^{+0.48}$  using the seismic moment conservation argument (Section 3).

The same type of analysis could be performed to estimate submarine landslide recurrence, though it is unclear what geologic factors are key to defining the ergodic ensemble. If there are multiple dates in a given region where the offshore sediment composition, tectonics, ground shaking, etc. are similar such as southern California, the age dates of multiple landslides within in the region can be grouped together to estimate the recurrence of landslides (Lee et al., 2004). For a global ensemble, however, one has to take into account differences in sediment (clastic vs. carbonate), tectonic movement (passive margin vs. active movement as in Puerto Rico), glacial activity, and peak ground acceleration. Too large of an ensemble can result in ergodicity breaking where the assumption no longer applies. This is discussed in the context of estimating uncertainty in the seismic attenuation relationship for earthquake ground motion studies by Anderson and Brune (1999). Lutz (2004) also indicates that physical systems that follow Lévy Law distributions (discussed below in terms of slip distributions) may also exhibit ergodicity breaking. While rigorously proving the ergodic assumption for complex systems is difficult, the assumption should at minimum be closely examined for specific situations to determine its domain of applicability.

#### 4.2 Incorporating Uncertainties into PTHA

Similar to PSHA, it is convenient to classify PTHA uncertainty as being epistemic or aleatory (Senior Seismic Hazard Analysis Committee (SSHAC), 1997; Toro et al., 1997; National Research Council (NRC), 2000). Epistemic uncertainty is also referred to as knowledge uncertainty that can be reduced by the collection of new data. Such uncertainty is often incorporated into probabilistic calculations through logic trees and computation of multiple hazard curves. From these, a mean or percentile hazard curve is determined, depending on the particular application (Abrahamson and Bommer, 2005; McGuire et al., 2005). An example of epistemic uncertainty is the mode of earthquake occurrence along the Aleutian-Alaskan subduction zone described by Wesson et al. (1999). In this case, two different segmentation models are considered involving both a G-R distribution of magnitudes and a characteristic mode of rupture at the site of the 1964 Alaska earthquake. These are associated with two different branches of a logic tree, each with specified weights, that are incorporated into computation of ground acceleration in the case of Wesson et al. (1999), and for tsunamis originating from the Aleutian-Alaskan subduction zone in the case of the Seaside, Oregon pilot study (Tsunami Pilot Study Working Group, 2006).

Aleatory uncertainty relates to the natural or stochastic uncertainty inherent in the physical system. Aleatory uncertainty is incorporated into probabilistic analysis through direct integration in the  $P(R > R_0 | \psi_{ij})$  term (equation 16). Recall that  $\psi_{ij}$  is the parameter(s) that is directly linked to the source frequency-size distribution. Other source parameters that result in a range of runup for a particular value of  $\psi_{ij}$  can be considered as random variables  $y_k$ ,  $k=1,2,3\dots$ . For a single random variable  $y$  where  $R(y)$  is normally distributed and has expected value ( $\mu_y$ ), and variance ( $\sigma_y^2$ ),

$$P(R(y) > R_0 | y) = \int_{R_0}^{\infty} \frac{1}{\sigma_y \sqrt{2\pi}} \exp\left(-\frac{1}{2} \frac{(R(y) - \mu_y)^2}{\sigma_y^2}\right) dR. \quad (34)$$

Multiple independent random variables ( $y_k$ ), each resulting in a normally distributed  $R(y_k)$ , will combine such that the aggregate pdf  $p(R | \psi_{i,j})$  is normally distributed according to the central limit theorem and under the conditions for which that theorem applies.

An example of how aleatory uncertainty is incorporated into PTHA calculations is described by Mofjeld et al. (2007) for the case of tsunami arrival time relative to tidal cycle. This is a non-trivial situation, since the tsunami wave train can extend over at least an entire tidal cycle. In this application, the pdf for the maximum tsunami wave height ( $\eta$ ) is a normal distribution that depends on the initial amplitude of the incident wave ( $A$ ) and a set of tidal constants ( $\kappa$ ):

$$p(\eta | A, \kappa) = \frac{1}{\sigma_\eta \sqrt{2\pi}} \exp\left(-\frac{1}{2} \frac{(\eta - \mu_\eta)^2}{\sigma_\eta^2}\right), \quad (35)$$

where

$$\mu_\eta = A + \text{MSL} + C(\text{MHHW} - \text{MSL}) \exp[-\alpha(A/\sigma_0)^\beta], \quad (36)$$

and

$$\sigma_\eta = \sigma_0 - C' \sigma_0 \exp[-\alpha'(A/\sigma_0)^\beta], \quad (37)$$

MSL and MHHW are mean sea level and mean higher high water, respectively,  $\sigma_0^2$  is the variance of the predicted tide, and  $C, C', \alpha, \alpha', \beta, \beta' \in \kappa$ , are all site specific constants (Mofjeld et al., 2007). The cumulative probability that the wave height will exceed a particular value ( $\eta_0$ ) over the entire duration of the tsunami is given by

$$P(\eta > \eta_0 | A, \kappa) = \int_{\eta_0}^{\infty} \frac{1}{\sigma_\eta \sqrt{2\pi}} \exp\left(-\frac{1}{2} \frac{(\eta - \mu_\eta)^2}{\sigma_\eta^2}\right) d\eta \quad (38)$$

Another example of aleatory uncertainty is variation in slip distribution patterns for an earthquake of a given magnitude. In this case, slip on a fault plane inclined below the surface of the earth  $u(\xi, y)$  (cf., Geist and Dmowska, 1999) is determined by specifying the slip spectrum in the radial wavenumber domain that can be directly linked to seismic observations (Hanks, 1979; Andrews, 1980; Frankel, 1991; Herrero and Bernard, 1994; Tsai, 1997; Somerville et al., 1999; Hisada, 2000; 2001; Mai and Beroza, 2002). Phase space is then randomized to yield a suite of  $u(\xi, y)$  distributions that correspond to the same scalar seismic moment and seismic source spectrum. The suite of  $u(\xi, y)$  can be used to estimate the uncertainty in local tsunami amplitude for a given seismic moment (Geist, 2002; 2005) as shown in Fig. 4.12 for a M~9 earthquake in the U.S. Pacific Northwest. In this case, the hazard variable is peak nearshore amplitude ( $A$ ) rather than runup. The distribution of tsunami incident amplitudes  $P(A > A_0 | u(\xi, y))$  arising from different slip distribution patterns is approximately a normal distribution, although there can be site-specific deviations owing to propagation path effects (Geist, 2005; Geist and Parsons, 2006).

For descriptive purposes, we can assign a random variable  $y_\phi$  that defines the phase space for the slip distribution  $u(\xi, y)$ . In most formulations of stochastic slip distributions (including Geist, 2002; 2005),  $y_\phi$  is assumed to be normally distributed. Recent research, however, indicates that the standard self-affine slip model described above may not accurately encompass possible large fluctuations in slip (Lavallée and Archuleta, 2003; Lavallée et al., 2006). The modification proposed by Lavallée et al. (2006) is to use the more general Lévy law distributions to describe  $y_\phi$ . (Lavallée et al., 2006, describes 1D and 2D stochastic modeling in more detail than the simple parameterization by  $y_\phi$  described here.) The Lévy law describes a class of stable distributions characterized by several parameters including the Lévy exponent  $\mu: 0 < \mu < 2$  (Sornette, 2004; Lavallée et al., 2006). Specific

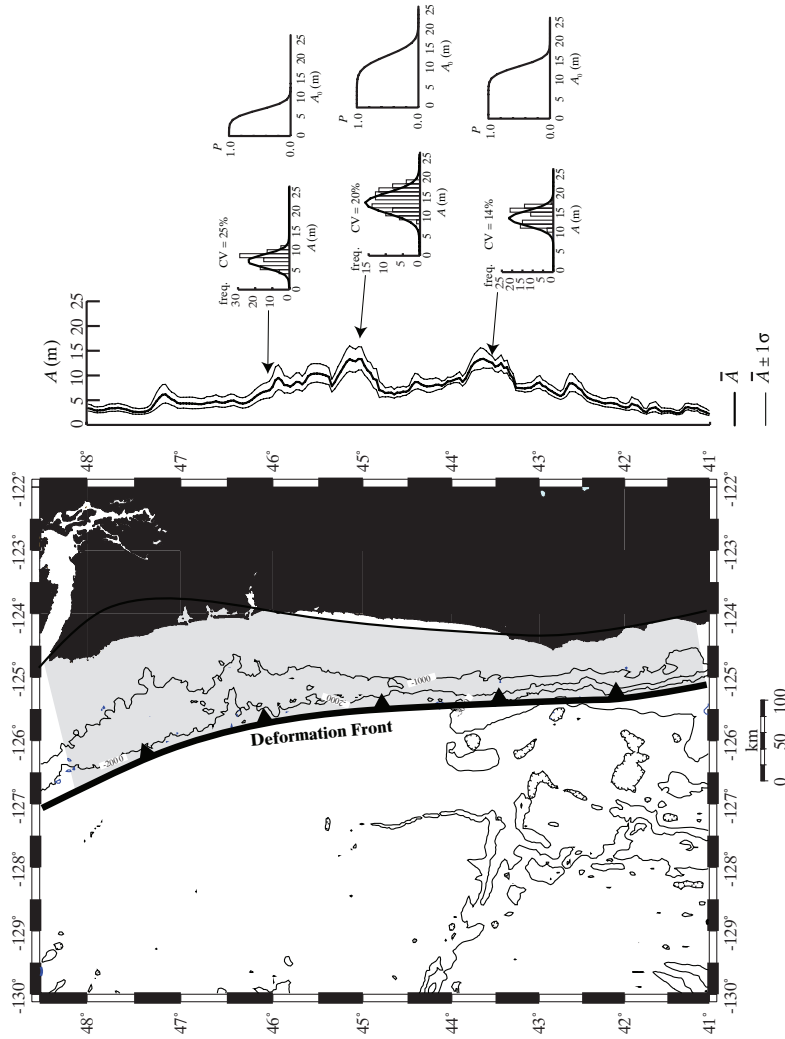


Fig. 4.12 – Example of how aleatory uncertainty in the earthquake source is integrated into the  $P$  term in equation 16. In this case for the U.S. Pacific Northwest, uncertainty of peak near shore tsunami amplitude ( $A$ ) from variations of slip distribution patterns for a local  $M \sim 9$  earthquake (shaded region) is determined from numerical tsunami propagation models. Left column of plots indicate histograms of  $A$  values and a normal distribution approximation (solid line). CV: coefficient of variation. Right column of plots indicates the function  $P(A > A_0 | u(\xi, y))$  using the cumulative normal distribution function (equation 34) for different threshold values,  $A_0$ . Details given by Geist and Parsons (2006).

analytic cases of symmetric Lévy distributions include the Cauchy-Lorentz distribution ( $\mu = 1$ ) and the Lévy distribution ( $\mu = 1/2$ ). Each of these are heavy tail pdf's in comparison to the normal distribution ( $\mu = 2$ ). Slip distributions determined from tsunami data collected during the 2004 Indian Ocean event (Fujii and Satake, 2007) suggest that this was a case of high slip fluctuation (Geist et al., 2007) and indicating that Lévy law distributions may need to be considered when estimating uncertainty of tsunami runup from distributed slip. Note that for the two examples of aleatory uncertainty described above,  $p(\eta | A, \kappa)$  and  $p(A | u(\xi, y))$  are obviously not independent, in that the distribution of combined tsunami and tidal wave heights are functionally dependent on  $A$  (Mofjeld et al., 2007).

As demonstrated by Geist and Parsons (2006), Monte Carlo methods are particularly useful for incorporating multiple sources of uncertainty. In this case, slip distribution, hypocenter (within the bounds specified by the seismogenic zone), and magnitude (taken from a sample of a seismic moment-balanced G-R distribution) all were randomized to yield a tsunami hazard curve at a particular coastal site. For the case of Acapulco, the computational curve compares well with the empirical curve determined from the available tsunami catalog data, when the limitations of the catalog are taken into account (Fig. 4.2).

### 4.3 Probabilities of Extreme Tsunamis

In some applications, it is necessary to determine the severity of an extreme event located at the tail of the tsunami frequency-size distribution. Issues such as knowing total insurance risk, economic impact, and long-term hazard for critical facilities necessitate estimating extreme values in natural hazards. However, there is a high level of uncertainty associated with these estimates, stemming from a lack of historical data and knowledge of what the maximum possible event may be.

#### Empirical Approach

A standard approach to such empirical problems is to use an asymptotic model of extremes, in which the cumulative distribution of the largest events approaches one of a member of the class of distributions called the General Extreme Value Distributions (GEVD) (Castillo et al., 2005). The basic members of the GEVD class include the Gumbel distribution (tail tapering off faster than a power law), Fréchet (tail tapering off as a power law), and Weibull (tail with finite right end point) (Kotz and Nadarajah, 2000; Sornette, 2004). Of the three, the Gumbel distribution (Gumbel, 1958) has been most often applied to natural hazards, since it has an infinite right tail but corresponds in general to a tapered power-law distribution. In particular, Hogben (1990) uses GEVD to determine extreme storm wave heights and Kulikov et al. (2005) presents a probabilistic analysis of tsunami hazards in Peru and northern Chile based on the Gumbel distribution.

The main problem with using the asymptotic models of extremes is that they do not make use of the full dataset or underlying pdf (Knopoff and Kagan, 1977; Sornette, 2004). Instead, rank-ordering statistics of an observed dataset (as in the Peaks-Over-Threshold modeling in extreme value theory) can be used to define the power-law exponent at extreme values (Knopoff and Kagan, 1977; Sornette et al., 1996). In addition, the generalized Pareto distribution (GPD) as described for earthquakes, floods, and extreme tides (Pugh, 1987; Stedinger et al., 1993; Pis-

arenko and Sornette, 2003) can be used to establish the extreme value distribution. The GPD is as follows:

$$G_{\xi,s}(x) = \begin{cases} 1 - (1 + \xi x/s)^{-1/\xi}, & \text{for } \xi \neq 0 \\ 1 - \exp(-x/s), & \text{for } \xi = 0 \end{cases} \quad (39)$$

where  $\xi$  is a shape parameter that is dependent on the pdf of the observations and  $s$  is a scale parameter which depends on the threshold of observations. Kijko (2004) also provides techniques to estimate the hard maximum limit  $R_x$ , whether or not the underlying distribution is known.

### Computational Approach

For the computational approach, one can follow the general method described in Section 4, paying careful attention to the underlying source-size distribution function and the attendant uncertainties. Of course, the analysis of extreme tsunamis greatly depends on the assumed mode of occurrence for the sources. For example, under the seismic gap hypothesis, the maximum size of a tsunami from a given fault segment is limited by the characteristic earthquake magnitude. This greatly reduces the uncertainty associated with determination of the maximum tsunamis, as does the assumption of a universal value for the aperiodicity parameter ( $\alpha$ ). However, a more realistic view of earthquake occurrence based on a soft-taper in the power-law distribution of sizes necessitates a more difficult analysis of uncertainties as described below.

In establishing the distribution of extreme source sizes, one can again use the GPD as described above or establish the corner seismic moment (earthquakes) or corner volume (landslides) using a modified power-law distribution. For the latter, parameter estimation of both  $M_c$  and  $\beta$  from global seismicity use the maximum likelihood method (e.g., Bird and Kagan, 2004). In this case the log-likelihood function ( $\ell$ ) for the tapered Pareto distribution (i.e., modified G-R distribution) is given by

$$\ell = \sum_{i=1}^n \log\left(\frac{\beta}{M_i} + \frac{1}{M_c}\right) + \beta n \log(M_t) - \beta \sum_{i=1}^n \log(M_i) + \frac{nM_t}{M_c} - \frac{1}{M_c} \sum_{i=1}^n M_i, \quad (40)$$

where  $M_i$  are  $i=1,2,3\dots n$  iid observations of seismic moment (cf., equations 17 and 18). In addition, Kagan and Schoenberg (2001) describe several other approaches to estimate the corner moment, including average likelihood estimates and a method of moments estimator. Pisarenko and Sornette (2003) argue that the shape parameter  $\xi$  of the GPD in equation 39 (estimate constrained by the Kolmogorov distance) is more tightly constrained than the corner moment.

Care must also be taken in how epistemic uncertainty in determining tsunami amplitudes from a particular extreme source is propagated through the calculations. One particular concern is determining which quantile curve is most representative of the hazard where there is significant epistemic uncertainty. This has been discussed recently for PSHA studies in comparing mean, median and fractile hazard curves by Abrahamson and Bommer (2005) derived from different

branches of an epistemic logic tree. They indicate that the mean hazard curve diverges significantly from the median hazard curve to higher hazard levels for very low hazard rates ( $10^{-7}$ - $10^{-8}$  yr<sup>-1</sup>). However McGuire et al. (2005) suggests that this is more of a problem with how the logic tree is formulated and weights assigned (cf., Senior Seismic Hazard Analysis Committee (SSHAC), 1997) and that the mean hazard curve is more in line with current understanding of the meaning of probability. Ideally, one would look at the entire probability distribution at a particular hazard level to determine how much information is contained in the probability estimate (Savage, 1991).

## 5. Summary

In this chapter, we have outlined empirical and computational approaches to estimate tsunami probability. Both approaches are centered around determining the frequency-size and inter-event time distributions. In the case of the empirical approach, these distributions apply to the tsunamis themselves, whereas in the computational approach, the distributions apply to the tsunami sources. Previous studies (e.g., Burroughs and Tebbens, 2005) have indicated that tsunami sizes are nominally distributed according to a power-law that is modified to include a taper or roll-off at large sizes. It is in fact uncertain what the limiting size of a tsunami is, since there are very low probability geologic processes that can theoretically produce much larger tsunamis than discussed here (e.g., catastrophic volcanic flank failures and asteroid impacts). In addition, there is likely a hydrodynamic limit for tsunami size, influenced by nonlinear shoaling effects and offshore wave breaking (Korycansky and Lynett, 2005). This chapter shows that for the inter-event time distribution, global tsunamis are characterized by a deviation from the exponential distribution associated with a Poisson process, especially at short inter-event times.

For the computational approach, the size distribution of earthquakes is better constrained than that for landslides and tsunamis themselves. Substantial progress has been made in determining the power-law exponent ( $\beta$ ) and corner moment for the earthquake size distribution. Moreover, recent studies (ten Brink et al., 2006a) have indicated that offshore landslides may also follow a modified power-law distribution of sizes, with  $\beta$  dependent on mechanical properties of the slide material. For inter-event time distributions, both time-independent (Poissonian) and time-dependent distributions are described for earthquakes. Aside from universal distributions recently proposed (Corral, 2004; Davidsen and Goltz, 2004; Molchan, 2005), fault-specific parameters for time-dependent probability models are in practice difficult to determine. This is a result of questionable underlying assumptions of earthquake rupture (e.g., characteristic, time-predictable) and the necessary number and precision of historic and pre-historic observations. The situation for offshore landslides is even more uncertain, as there is a general lack of age dates for individual events. While we await more data to constrain the inter-event distributions, the null hypothesis of an exponential distribution is likely our best model.

Reducing sources of epistemic uncertainty is key to developing more accurate tsunami probability estimates for the computational approach in the future. While most tsunami source parameters are approximately normally distributed, there are some parameters such as landslide speed where there is insufficient data to make

this assumption. In addition, other parameters such as slip distribution appear to exhibit stronger fluctuations than expected from a normal distribution (Lavallée et al., 2006). Further research is needed to better quantify uncertainty for source parameters that scale with source size. For any tsunami probability study, it is important to understand how uncertainty affects the probability estimate, either through a determination of information content (Savage, 1991; 1992) or through Monte Carlo techniques (Parsons, 2004; 2005).

### Acknowledgements

The authors gratefully acknowledge constructive reviews of this chapter by David Divoky, Hal Mofjeld, Hong Kie Thio, and Annabel Kelly. James Savage also provided helpful comments related to empirical probability.

### References

- Abe, K., 1995. Estimate of tsunami run-up heights from earthquake magnitudes. In: Y. Tsuchiya and N. Shuto (Editors), *Tsunami: Progress in Prediction, Disaster Prevention and Warning*, v. 4. Kluwer Academic Publishers, Dordrecht, pp. 21–35.
- Abrahamson, N. A. and Bommer, J. J., 2005. Probability and uncertainty in seismic hazard analysis. *Earthquake Spectra*, 21, 603–607.
- Altmann, E. G. and Kantz, H., 2005. Recurrence time analysis, long-term correlations, and extreme events. *Physical Review E*, 71, doi: 10.1103/PhysRevE.71.056106.
- Anderson, J. G. and Brune, J. N., 1999. Probabilistic seismic hazard analysis without the ergodic assumption. *Seismological Research Letters*, 70, 19–28.
- Andrews, D. J., 1980. A stochastic fault model 1. Static case. *Journal of Geophysical Research*, 85, 3867–3877.
- Anosov, D. V., 2001. Ergodic Theory. In: M. Hazewinkel (Editor), *Encyclopaedia of Mathematics*. Springer-Verlag, Berlin, pp. <http://eom.springer.de/e/e036150.htm>.
- Atwater, B. F., Tuttle, M. P., Schweig, E. S., Rubin, C. M., Yamaguchi, D. K. and Hemphill-Haley, E., 2004. Earthquake recurrence inferred from paleoseismology. *Developments in Quaternary Science*, 1, 331–350.
- Bak, P., Christensen, K., Danon, L. and Scanlon, T., 2002. Unified scaling law for earthquakes. *Physical Review Letters*, 88, doi: 10.1103/PhysRevLett.88.178501.
- Beichelt, F. E. and Fatti, L. P., 2002. *Stochastic processes and their applications*. Taylor & Francis, London, 326 pp.
- Ben-Menahem, A. and Rosenman, M., 1972. Amplitude patterns of tsunami waves from submarine earthquakes. *Journal of Geophysical Research*, 77, 3097–3128.
- Ben-Zion, Y., 1996. Stress, slip, and earthquakes in models of complex single-fault systems incorporating brittle and creep deformations. *Journal of Geophysical Research*, 101, 5677–5706.
- Ben-Zion, Y. and Rice, J. R., 1997. Dynamic simulations of slip on a smooth fault in an elastic solid. *Journal of Geophysical Research*, 102, 17,771–17,784.
- Bird, P., 2003. An updated digital model of plate boundaries. *Geochemistry, Geophysics, Geosystems*, 4, doi:10.1029/2001GC000252.
- Bird, P. and Kagan, Y. Y., 2004. Plate-tectonic analysis of shallow seismicity: apparent boundary width, beta-value, corner magnitude, coupled lithosphere thickness, and coupling in 7 tectonic settings. *Bulletin of the Seismological Society of America*, 94, 2380–2399.

- Biscontin, G. and Pestana, J. M., 2006. Factors affecting seismic response of submarine slopes. *Natural Hazards and Earth System Sciences*, 6, 97–107.
- Biscontin, G., Pestana, J. M. and Nadim, F., 2004. Seismic triggering of submarine slides in soft cohesive soil deposits. *Marine Geology*, 203, 341–354.
- Bronk Ramsey, C., 1998. Probability and dating. *Radiocarbon*, 40, 461–474.
- Burroughs, S. M. and Tebbens, S. F., 2001. Upper-truncated power laws in natural systems. *Pure and Applied Geophysics*, 158, 741–757.
- Burroughs, S. M. and Tebbens, S. F., 2005. Power law scaling and probabilistic forecasting of tsunami runup heights. *Pure and Applied Geophysics*, 162, 331–342.
- Caldwell, P. and Merrifield, M. A., 2006. Joint archive for sea level data report: March 2006. JIMAR Contribution No. 06-360, Data Report No. 19.
- Castillo, E., Hadi, A. S., Balakrishnan, N. and Sarabia, J. M., 2005. *Extreme Value and Related Models with Applications in Engineering and Science*. Wiley Series in Probability and Statistics. John Wiley & Sons, Inc., Hoboken, NJ, 362 pp.
- Cochar, A. and Madariaga, R., 1996. Complexity of seismicity due to highly rate dependent friction. *Journal of Geophysical Research*, 101, 25,321–25,336.
- Conover, W. J., 1971. *Practical Nonparametric Statistics*. John Wiley and Sons Inc., New York, 462 pp.
- Cornell, C. A., 1968. Engineering seismic risk analysis. *Bulletin of the Seismological Society of America*, 58, 1583–1606.
- Corral, A., 2004. Long-term clustering, scaling, and universality in the temporal occurrence of earthquakes. *Physical Review Letters*, 92, doi: 10.1103/PhysRevLett.92.108501.
- Corral, A., 2005a. Mixing of rescaled data and Bayesian inference for earthquake recurrence times. *Nonlinear Processes in Geophysics*, 12, 89–100.
- Corral, A., 2005b. Statistical features of earthquake temporal occurrence. In: B. K. Chakrabarti and P. Bhattacharyya (Editors), *International Workshop on Models of Earthquakes: Physics Approaches*, Calcutta, India.
- Corral, A., 2005c. Time-decreasing hazard and increasing time until the next earthquake. *Physical Review E*, 71, doi: 10.1103/PhysRevE.71.017101.
- Daley, D. J. and Vere-Jones, D., 2003. *An Introduction to the Theory of Point Processes*, 1. Springer, New York, 469 pp.
- Daley, D. J. and Vere-Jones, D., 2004. Scoring probability forecasts for point processes: The entropy score and information gain. *Journal of Applied Probability*, 41A, 297–312.
- Davidson, J. and Goltz, C., 2004. Are seismic waiting time distributions universal? *Geophysical Research Letters*, 31, doi: 10.1029/2004GL020892.
- Davis, P. M., Jackson, D. D. and Kagan, Y. Y., 1989. The longer it has been since the last earthquake, the longer the expected time till the next? *Bulletin of the Seismological Society of America*, 79, 1439–1456.
- Densmore, A. L., Ellis, M. A. and Anderson, R. S., 1998. Landsliding and the evolution of normal-fault-bounded mountains. *Journal of Geophysical Research*, 103, 15,203–15,219.
- Dugan, B. and Flemings, P. B., 2000. Overpressure and fluid flow in the New Jersey continental slope: Implications for slope failure and cold seeps. *Science*, 289, 288–291.
- Dussauge, C., Grasso, J. R. and Helmstetter, A., 2003. Statistical analysis of rockfall volume distributions: Implications for rockfall dynamics. *Journal of Geophysical Research*, 108, doi:10.1029/2001JB000650.
- Finkelstein, J. M. and Schafer, R. E., 1971. Improved goodness-of-fit tests. *Biometrika*, 58, 641–645.
- Fisher, M. A., Normark, W. R., Greene, H. G., Lee, H. J. and Sliter, R. W., 2005. Geology and tsunami-genic potential of submarine landslides in Santa Barbara Channel, southern California. *Marine Geology*, 224, 1–22.

- Flinn, E. A., Engdahl, E. R. and Hill, A. R., 1974. Seismic and geographical regionalization. *Bulletin of the Seismological Society of America*, 64, 771–992.
- Frankel, A. D., 1991. High-frequency spectral falloff of earthquakes, fractal dimension of complex rupture,  $b$  value, and the scaling of strength on faults. *Journal of Geophysical Research*, 96, 6291–6302.
- Frankel, A. D., Petersen, M. D., Mueller, C. S., Haller, K. M., Wheeler, R. L., Leyendecker, E. V., Wesson, R. L., Harmsen, S. C., Cramer, C. H., Perkins, D. M. and Rukstales, K. S., 2002. Documentation for the 2002 Update of the National Seismic Hazard Maps. Open-File Report 02-420, U.S. Geological Survey.
- Fujii, Y. and Satake, K., 2007. Tsunami source of the 2004 Sumatra-Andaman earthquake inferred from tide gauge and satellite data. *Bulletin of the Seismological Society of America*, 97, S192-S207.
- Geist, E. L., 1999. Local tsunamis and earthquake source parameters. *Advances in Geophysics*, 39, 117–209.
- Geist, E. L., 2002. Complex earthquake rupture and local tsunamis. *Journal of Geophysical Research*, 107, doi:10.1029/2000JB000139.
- Geist, E. L., 2005. Local Tsunami Hazards in the Pacific Northwest from Cascadia Subduction Zone Earthquakes. U.S. Geological Survey Professional Paper 1661B.
- Geist, E. L. and Dmowska, R., 1999. Local tsunamis and distributed slip at the source. *Pure and Applied Geophysics*, 154, 485–512.
- Geist, E. L. and Parsons, T., 2005. Triggering of Tsunamiogenic Aftershocks from Large Strike-Slip Earthquakes: Analysis of the November 2000 New Ireland Earthquake Sequence. *Geochemistry, Geophysics, Geosystems*, 6(Q10005), doi:10.1029/2005GC000935.
- Geist, E. L. and Parsons, T., 2006. Probabilistic analysis of tsunami hazards. *Natural Hazards*, 37, 277–314.
- Geist, E. L. and Parsons, T., in press. Distribution of tsunami inter-Event times. *Geophysical Research Letters*.
- Geist, E. L., Titov, V. V., Arcas, D., Pollitz, F. F. and Bilek, S. L., 2007. Implications of the December 26, 2004 Sumatra-Andaman earthquake on tsunami forecast and assessment models for great subduction zone earthquakes. *Bulletin of the Seismological Society of America*, 97, S249-S270.
- Gisler, G., Weaver, R. and Gittings, M. L., 2006. SAGE calculations of the tsunami threat from La Palma. *Science of Tsunami Hazards*, 24, 288–301.
- Gumbel, E. J., 1958. *Statistics of Extremes*. Columbia University Press, New York, 375 pp.
- Guzzetti, F., Malamud, B. D., Turcotte, D. L. and Reichenbach, P., 2002. Power-law correlations of landslide areas in central Italy. *Earth and Planetary Science Letters*, 195, 169–183.
- Hanks, T. C., 1979.  $b$  values and  $\omega^{\gamma}$  seismic source models: Implications for tectonic stress variations along active crustal fault zones and the estimation of high-frequency strong ground motion. *Journal of Geophysical Research*, 84, 2235–2242.
- Hanks, T. C. and Kanamori, H., 1979. A moment magnitude scale. *Journal of Geophysical Research*, 84, 2348–2350.
- Harte, D. and Vere-Jones, D., 2005. The entropy score and its uses in earthquake forecasting. *Pure and Applied Geophysics*, 162, 1229–1253.
- Heinrich, P., Piatanesi, A. and Hébert, H., 2001. Numerical modelling of tsunami generation and propagation from submarine slumps: the 1998 Papua New Guinea event. *Geophysical Journal International*, 145, 97–111.
- Hergarten, S., 2003. Landslides, sandpiles, and self-organized criticality. *Natural Hazards and Earth System Sciences*, 3, 505–514.
- Hergarten, S. and Neugebauer, H. J., 1998. Self-organized criticality in a landslide model. *Geophysical Research Letters*, 25, 801–804.

- Herrero, A. and Bernard, P., 1994. A kinematic self-similar rupture process for earthquakes. *Bulletin of the Seismological Society of America*, 84, 1216–1228.
- Hino, R., Tanioka, Y., Kanazawa, T., Sakai, S., Nishino, M. and Suyehiro, K., 2001. Micro-tsunami from a local interplate earthquake detected by cabled offshore tsunami observation in northeastern Japan. *Geophysical Research Letters*, 28, 3533–3536.
- Hirata, K., Takahashi, H., Geist, E. L., Satake, K., Tanioka, Y., Sugioka, H. and Mikada, H., 2003. Source depth dependence of micro-tsunamis recorded with ocean-bottom pressure gauges; the January 28, 2000 Mw 6.8 earthquake off Nemuro Peninsula, Japan. *Earth and Planetary Science Letters*, 208(3–4), 305–318.
- Hisada, Y., 2000. A theoretical omega-square model considering the spatial variation in slip and rupture velocity. *Bulletin of the Seismological Society of America*, 90, 387–400.
- Hisada, Y., 2001. A theoretical omega-square model considering the spatial variation in slip and rupture velocity. Part 2: Case for a two-dimensional source model. *Bulletin of the Seismological Society of America*, 91, 651–666.
- Hogben, N., 1990. Long term wave statistics. In: B. Le Méhauté and D. M. Hanes (Editors), *Ocean Engineering Science. The Sea*, v. 9. John Wiley & Sons, New York, pp. 293–333.
- Houston, J. R. and Garcia, A. W., 1978. Type 16 Flood Insurance Study: Tsunami Predictions for the West Coast of the Continental United States. Technical Report H-78-26, U.S. Army Engineer Waterways Experiment Station, Vicksburg, MS.
- Howell, B. F., 1985. On the effect of too small a data base on earthquake frequency diagrams. *Bulletin of the Seismological Society of America*, 75, 1205–1207.
- Howson, C. and Urbach, P., 1993. *Scientific Reasoning: The Bayesian Approach*. Open Court Publishing Company, Chicago, Illinois, 470 pp.
- Hutton, E. W. H. and Syvitski, J. P. M., 2004. Advances in the numerical modeling of sediment failure during the development of a continental margin. *Marine Geology*, 203, 367–380.
- Issler, D., De Blasio, F. V., Elverhøi, A., Bryn, P. and Lien, R., 2005. Scaling behaviour of clay-rich submarine debris flows. *Marine and Petroleum Geology*, 22, 187–194.
- Jaynes, E. T., 2003. *Probability Theory: The Logic of Science*. Cambridge University Press, Cambridge, UK, 727 pp.
- Jiang, L. and Leblond, P. H., 1994. Three-dimensional modeling of tsunami generation due to a submarine mudslide. *Journal of Physical Oceanography*, 24, 559–572.
- Kagan, Y. Y., 1993. Statistics of characteristic earthquakes. *Bulletin of the Seismological Society of America*, 83, 7–24.
- Kagan, Y. Y., 1997. Seismic moment-frequency relation for shallow earthquakes: Regional comparison. *Journal of Geophysical Research*, 102, 2835–2852.
- Kagan, Y. Y., 1999. Universality of the seismic-moment-frequency relation. *Pure and Applied Geophysics*, 155, 537–573.
- Kagan, Y. Y., 2002a. Seismic moment distribution revisited: I. Statistical Results. *Geophysical Journal International*, 148, 520–541.
- Kagan, Y. Y., 2002b. Seismic moment distribution revisited: II. Moment conservation principle. *Geophysical Journal International*, 149, 731–754.
- Kagan, Y. Y. and Jackson, D. D., 1991. Seismic gap hypothesis: Ten years after. *Journal of Geophysical Research*, 96, 21,419–21,431.
- Kagan, Y. Y. and Jackson, D. D., 1995. New seismic gap hypothesis: Five years after. *Journal of Geophysical Research*, 100, 3943–3959.
- Kagan, Y. Y. and Jackson, D. D., 2000. Probabilistic forecasting of earthquakes. *Geophysical Journal International*, 143, 438–453.
- Kagan, Y. Y. and Schoenberg, F., 2001. Estimation of the upper cutoff parameter for the tapered Pareto distribution. *Journal of Applied Probability*, 38A, 158–175.

- Kajiura, K., 1981. Tsunami energy in relation to parameters of the earthquake fault model. *Bulletin of the Earthquake Research Institute*, 56, 415–440.
- Keefer, D. K., 1994. The importance of earthquake-induced landslides to long-term slope erosion and slope-failure hazards in seismically active regions. *Geomorphology*, 10, 265–284.
- Kempthorne, O. and Folks, L., 1971. *Probability, Statistics, and Data Analysis*. Iowa State University Press, Ames, Iowa, 555 pp.
- Kijko, A., 2004. Estimation of the maximum earthquake magnitude,  $m_{\max}$ . *Pure and Applied Geophysics*, 161, 1655–1681.
- Knopoff, L. and Kagan, Y. Y., 1977. Analysis of the theory of extremes as applied to earthquake problems. *Journal of Geophysical Research*, 82, 5647–5657.
- Korycansky, D. G. and Lynett, P. J., 2005. Offshore breaking of impact tsunami: The Van Dorn effect revisited. *Geophysical Research Letters*, 32, doi:10.1029/2004GL021918.
- Kotz, S. and Nadarajah, S., 2000. *Extreme Value Distributions: Theory and Applications*. Imperial College Press, London, 187 pp.
- Kreemer, C., Holt, W. E. and Haines, A. J., 2003. An integrated global model of present-day plate motions and plate boundary deformation. *Geophysical Journal International*, 154, 8–34.
- Kulikov, E. A., Rabinovich, A. B. and Thomson, R., 2005. Estimation of tsunami risk for the coasts of Peru and northern Chile. *Natural Hazards*, 35, 185–209.
- Lavallée, D. and Archuleta, R. J., 2003. Stochastic modeling of slip spatial complexities for the 1979 Imperial Valley, California, earthquake. *Geophysical Research Letters*, 30, doi:10.1029/2002GL015839.
- Lavallée, D., Liu, P. and Archuleta, R. J., 2006. Stochastic model of heterogeneity in earthquake slip spatial distributions. *Geophysical Journal International*, 165, 622–640.
- Lee, H., Normark, W. R., Fisher, M. A., Greene, H. G., Edwards, B. D. and Locat, J., 2004. Timing and extent of submarine landslides in southern California, Offshore Technology Conference, Houston, Texas, U.S.A., pp. OTC Paper Number 16744.
- Lee, H. J., 2005. Undersea landslides: extent and significance in the Pacific Ocean, an update. *Natural Hazards and Earth System Sciences*, 5, 877–892.
- Lin, I. and Tung, C. C., 1982. A preliminary investigation of tsunami hazard. *Bulletin of the Seismological Society of America*, 72, 2323–2337.
- Liu, P. L. F., Wu, T.-R., Raichlen, F., Synolakis, C. E. and Borrero, J. C., 2005. Runup and rundown generated by three-dimensional sliding masses. *Journal of Fluid Mechanics*, 536, 107–144.
- Locat, J. and Lee, H. J., 2002. Submarine landslides: advances and challenges. *Canadian Geotechnical Journal*, 39, 193–212.
- Locat, J., Lee, H. J., Locat, P. and Imran, J., 2004. Numerical analysis of the mobility of the Palos Verdes debris avalanche, California, and its implication for the generation of tsunamis. *Marine Geology*, 203, 269–280.
- Lomnitz, C. and Nava, F. A., 1983. The predictive value of seismic gaps. *Bulletin of the Seismological Society of America*, 73, 1815–1824.
- Lu, C. and Vere-Jones, D., 2001. Statistical analysis of synthetic earthquake catalogs generated by models with various levels of fault zone disorder. *Journal of Geophysical Research*, 106, 11,115–11,125.
- Lutz, E., 2004. Power-law tail distributions and nonergodicity. *Physical Review Letters*, 93, doi:10.1103/PhysRevLett.93.190602.
- Mai, P. M. and Beroza, G. C., 2002. A spatial random field model to characterize complexity in earthquake slip. *Journal of Geophysical Research*, 107, doi:10.1029/2001JB000588.
- Malamud, B. D., Turcotte, D. L., Guzzetti, F. and Reichenbach, P., 2004. Landslide inventories and their statistical properties. *Earth Surface Processes and Landforms*, 29, 687–711.

- Marsan, D., 2005. The role of small earthquakes in redistributing crustal elastic stress. *Geophysical Journal International*, 163, 141–151.
- Matthews, M. V., Ellsworth, W. L. and Reasenber, P. A., 2002. A Brownian model for recurrent earthquakes. *Bulletin of the Seismological Society of America*, 92, 2233–2250.
- McCann, W. R., Nishenko, S. P., Sykes, L. R. and Krause, J., 1979. Seismic gaps and plate tectonics: seismic potential for major boundaries. *Pure and Applied Geophysics*, 117, 1082–1147.
- McGuire, R. K., Cornell, C. A. and Toro, G. R., 2005. The case for using mean seismic hazard. *Earthquake Spectra*, 21, 879–886.
- Michael, A. J., 2005. Viscoelasticity, postseismic slip, fault interactions, and the recurrence of large earthquakes. *Bulletin of the Seismological Society of America*, 95, 1594–1603.
- Mofjeld, H. O., González, F. I., Titov, V. V., Venturato, A. J. and Newman, A. V., 2007. Effects of tides on maximum tsunami wave heights: Probability distributions. *Journal of Atmospheric and Oceanic Technology*, 24, 117–123.
- Molchan, G., 2005. Interevent time distribution in seismicity: A theoretical approach. *Pure and Applied Geophysics*, 162, 1135–1150.
- Murray, J. and Segall, P., 2002. Testing time-predictable earthquake recurrence by direct measurement of strain accumulation and release. *Nature*, 419, 287–291.
- National Research Council (NRC), 2000. *Risk Analysis and Uncertainty in Flood Damage Reduction Studies*. National Academy Press, Washington, DC, 202 pp.
- Nishenko, S. P., 1991. Circum-Pacific seismic potential: 1989–1999. *Pure and Applied Geophysics*, 135, 169–259.
- Nishenko, S. P. and Buland, R., 1987. A generic recurrence interval distribution for earthquake forecasting. *Bulletin of the Seismological Society of America*, 77, 1382–1399.
- Normark, W. R., McGann, M. and Sliter, R. W., 2004. Age of Palos Verdes submarine debris avalanche, southern California. *Marine Geology*, 203, 247–259.
- Ogata, Y., 1999. Estimating the hazard of rupture using uncertain occurrence times of paleoearthquakes. *Journal of Geophysical Research*, 104, 17,995–18,014.
- Okada, Y., 1985. Surface deformation due to shear and tensile faults in a half-space. *Bulletin of the Seismological Society of America*, 75, 1135–1154.
- Okal, E. A., 1988. Seismic parameters controlling far-field tsunami amplitudes: A review. *Natural Hazards*, 1, 67–96.
- Parsons, T., 2002. Global Omori law decay of triggered earthquakes: Large aftershocks outside the classical aftershock zone. *Journal of Geophysical Research*, 107, 2199, doi:10.1029/2001JB000646.
- Parsons, T., 2004. Recalculated probability of  $M \geq 7$  earthquakes beneath the Sea of Marmara, Turkey. *Journal of Geophysical Research*, 109, B05304.
- Parsons, T., 2005. Significance of stress transfer in time-dependent earthquake probability calculations. *Journal of Geophysical Research*, 110, doi:10.1029/2004JB003190.
- Parsons, T., 2006.  $M \geq 7.0$  earthquake recurrence on the San Andreas fault from a stress renewal model. *Journal of Geophysical Research*, 111, doi:10.1029/2006JB004415.
- Pelayo, A. M. and Wiens, D. A., 1992. Tsunami earthquakes: Slow thrust-faulting events in the accretionary wedge. *Journal of Geophysical Research*, 97, 15,321–15,337.
- Perfettini, H., Schmittbuhl, J. and Vilotte, J. P., 2001. Slip correlations on a creeping fault. *Geophysical Research Letters*, 28, 2137–2140.
- Pisarenko, V. F. and Sornette, D., 2003. Characterization of the frequency of extreme earthquake events by the Generalized Pareto Distribution. *Pure and Applied Geophysics*, 160, 2343–2364.
- Pugh, D. T., 1987. *Tides, Surges and Mean Sea-Level*. John Wiley & Sons, Chichester, UK, 472 pp.

- Rikitake, T., 1999. Probability of a great earthquake to recur in the Tokai district, Japan: reevaluation based on newly-developed paleoseismology, plate tectonics, tsunami study, micro-seismicity and geotectonic measurements. *Earth Planets Space*, 51, 147–157.
- Rikitake, T. and Aida, I., 1988. Tsunami hazard probability in Japan. *Bulletin of the Seismological Society of America*, 78, 1268–1278.
- Rong, Y., Jackson, D. D. and Kagan, Y. Y., 2003. Seismic gaps and earthquakes. *Journal of Geophysical Research*, 108, ESE 6-1 - 6-14.
- Satake, K., 2002. Tsunamis. In: W. H. K. Lee, H. Kanamori, P. C. Jennings and C. Kisslinger (Editors), *International Handbook of Earthquake and Engineering Seismology, Part A*. Academic Press, San Diego, pp. 437–451.
- Savage, J. C., 1991. Criticism of some forecasts of the National Earthquake Prediction Evaluation Council. *Bulletin of the Seismological Society of America*, 81, 862–881.
- Savage, J. C., 1992. The uncertainty in earthquake conditional probabilities. *Geophysical Research Letters*, 19, 709–712.
- Savage, J. C., 1994. Empirical earthquake probabilities from observed recurrence intervals. *Bulletin of the Seismological Society of America*, 84, 219–221.
- Senior Seismic Hazard Analysis Committee (SSHAC), 1997. Recommendations for Probabilistic Seismic Hazard Analysis: Guidance on Uncertainty and Use of Experts. Main Report NUREG/CR-6372 UCRL-ID-122160 Vol. 1, U.S. Nuclear Regulatory Commission.
- Shaw, B. E., 2004. Dynamic heterogeneities versus fixed heterogeneities in earthquake models. *Geophysical Journal International*, 156, 275–286.
- Shaw, B. E. and Rice, J. R., 2000. Existence of continuum complexity in the elastodynamics of repeated fault ruptures. *Journal of Geophysical Research*, 105, 23,791–23,810.
- Shimazaki, K. and Nakata, T., 1980. Time-predictable recurrence model for large earthquakes. *Geophysical Research Letters*, 7, 279–282.
- Shuto, N., 1991. Numerical simulation of tsunamis—Its present and near future. *Natural Hazards*, 4, 171–191.
- Solheim, A., Berg, K., Forsber, C. F. and Bryn, P., 2005a. The Storegga Slide complex: repetitive large scale sliding with similar cause and development. *Marine and Petroleum Geology*, 22, 97–107.
- Solheim, A., Bryn, P., Sejrup, H. P., Mienert, J. and Berg, K., 2005b. Ormen Lange—an integrated study for the safe development of a deep-water gas field within the Storegga Slide Complex, NE Atlantic continental margin: executive summary. *Marine and Petroleum Geology*, 22, 1–9.
- Somerville, P., Irikura, K., Graves, R., Sawada, S., Wald, D., Abrahamson, N. A., Iwasaki, Y., Kagawa, T., Smith, N. and Kowada, A., 1999. Characterizing crustal earthquake slip models for the prediction of strong ground motion. *Seismological Research Letters*, 70, 59–80.
- Sornette, D., 2004. *Critical Phenomena in Natural Sciences*. Springer Series in Synergetics. Springer-Verlag, Berlin, 528 pp.
- Sornette, D., Knopoff, L., Kagan, Y. Y. and Vanneste, C., 1996. Rank-ordering statistic of extreme events: Application to the distribution of large earthquakes. *Journal of Geophysical Research*, 101, 13,883–13,893.
- Stark, C. P. and Hovius, N., 2001. The characterization of landslide size distributions. *Geophysical Research Letters*, 28, 1091–1094.
- Stedinger, J. R., Vogel, R. M. and Foufoula-Georgiou, E., 1993. Frequency analysis of extreme events. In: D. R. Maidment (Editor), *Handbook of Hydrology*. McGraw Hill, Inc., New York, pp. 18.1–18.66.
- Stein, S. and Newman, A., 2004. Characteristic and uncharacteristic earthquakes as possible artifacts: Applications to the New Madrid and Wabash seismic zones. *Seismological Research Letters*, 75, 173–187.
- Stephens, M. A., 1974. EDF statistics for goodness of fit and some comparisons. *Journal of the American Statistical Association*, 69, 730–737.

- Tanioka, Y. and Satake, K., 1996. Tsunami generation by horizontal displacement of ocean bottom. *Geophysical Research Letters*, 23, 861–865.
- ten Brink, U. S., Geist, E. L. and Andrews, B. D., 2006a. Size distribution of submarine landslides and its implication to tsunami hazard in Puerto Rico. *Geophysical Research Letters*, 33, doi:10.1029/2006GL026125.
- ten Brink, U. S., Geist, E. L., Lynett, P. J. and Andrews, B. D., 2006b. Submarine slides north of Puerto Rico and their tsunami potential. In: A. Mercado and P. Liu (Editors), *Caribbean Tsunami Hazard*. World Scientific, Singapore, pp. 67–90.
- Thio, H. K., Ichinose, G., Polet, J. and Somerville, P., 2007. Application of probabilistic tsunami hazard analysis to ports and harbors, *Ports 2007*. American Society of Civil Engineers, San Diego.
- Todorovska, M. I., Hayir, A. and Trifunac, M. D., 2002. A note on tsunami amplitudes above submarine slides and slumps. *Soil Dynamics and Earthquake Engineering*, 22, 129–141.
- Toro, G. R., Abrahamson, N. A. and Schneider, J. F., 1997. Model of strong ground motions from earthquakes in central and eastern North America: Best estimates and uncertainties. *Seismological Research Letters*, 68, 41–57.
- Trifunac, M. D., Hayir, A. and Todorovska, M. I., 2002. A note on the effects of nonuniform spreading velocity of submarine slumps and slides on the near-field tsunami amplitudes. *Soil Dynamics and Earthquake Engineering*, 22, 167–180.
- Trifunac, M. D., Hayir, A. and Todorovska, M. I., 2003. A note on tsunami caused by submarine slides and slumps spreading in one dimension with nonuniform displacement amplitudes. *Soil Dynamics and Earthquake Engineering*, 23, 223–234.
- Tsai, C. P., 1997. Slip, stress drop and ground motion of earthquakes: A view from the perspective of fractional Brownian motion. *Pure and Applied Geophysics*, 149, 689–706.
- Tsunami Pilot Study Working Group, 2006. Seaside, Oregon Tsunami Pilot Study—Modernization of FEMA Flood Hazard Maps. Open-File Report 2006-1234, U. S. Geological Survey, <http://pubs.usgs.gov/of/2006/1234/>.
- Utsu, T., 1984. Estimation of parameters for recurrence models of earthquakes. *Bulletin of the Earthquake Research Institute*, 59, 53–66.
- Varnes, D. J., 1978. Slope movement types and processes. In: R. L. Schuster and R. J. Krizek (Editors), *Landslides: Analysis and Control*. National Academy of Sciences, Washington, D.C., pp. 11–33.
- Vere-Jones, D. and Ogata, Y., 2003. Statistical principles for seismologists. In: W. H. K. Lee, H. Kanamori, P. C. Jennings and C. Kisslinger (Editors), *International Handbook of Earthquake & Engineering Seismology, Part B*. Academic Press, pp. 1573–1586.
- Vere-Jones, D., Robinson, R. and Yang, W., 2001. Remarks on the accelerated moment release model: problems of model formulation, simulation and estimation. *Geophysical Journal International*, 144, 517–531.
- Ward, S. N., 1994. A multidisciplinary approach to seismic hazard in southern California. *Bulletin of the Seismological Society of America*, 84, 1293–1309.
- Ward, S. N., 2001. Landslide tsunami. *Journal of Geophysical Research*, 106, 11,201–11,215.
- Ward, S. N., 2002. Tsunamis. In: R. A. Meyers (Editor), *The Encyclopedia of Physical Science and Technology*, v. 17. Academic Press, pp. 175–191.
- Weldon, R. J., Fumal, T. E., Biasi, G. P. and Scharer, K. M., 2005. Past and future earthquakes on the San Andreas fault. *Science*, 308, 966–967.
- Weldon, R. J., Scharer, K. M., Fumal, T. E. and Biasi, G. P., 2004. Wrightwood and the earthquake cycle: What a long recurrence record tells us about how faults work. *GSA Today*, 14, doi:10.1130/1052-5173(2004)014.
- Wesnowsky, S. G., 1994. The Gutenberg-Richter or characteristic earthquake distribution, which is it? *Bulletin of the Seismological Society of America*, 84, 1940–1959.

- Wesson, R. L., Frankel, A. D., Mueller, C. S. and Harmsen, S. C., 1999. Probabilistic Seismic Hazard Maps of Alaska. Open-File Report 99-36, U.S. Geological Survey.
- Working Group on California Earthquake Probabilities, 1995. Seismic hazards in southern California: Probable earthquakes, 1994–2024. *Bulletin of the Seismological Society of America*, 85, 379–439.
- Yoshioka, S., Hashimoto, M. and Hirahara, K., 1989. Displacement fields due to the 1946 Nankaido earthquake in a laterally inhomogeneous structure with the subducting Philippine Sea plate—a three-dimensional finite element approach. *Tectonophysics*, 159, 121–136.
- Zeng, J. L., Heaton, T. H. and DiCaprio, C., 2005. The effect of slip variability on earthquake slip-length scaling. *Geophysical Journal International*, 162, 841–849.

